의학박사 학위논문

VISTA 발현 콩팥 거주 대식세포의 신장 손상에 대한 보호기전 연구

Study on the protective effect of VISTA–positive kidney resident macrophages against renal injury

2021 년 2 월

서울대학교 대학원
의과학과
의과학 전공

박준규

VISTA 발현 콩팥 거주 대식세포의 신장 손상에 대한 보호기전 연구

지도 교수 이 동 섭

이 논문을 이학박사 학위논문으로 제출함

2020년 10월

서울대학교 대학원
의과학과
의과학전공

박 준 규

박준규의 박사 학위논문을 인준함
2021년 1월

위원장 김 황 래 (인)
부위원장 이 동 섭 (인)
위원 최 은 영 (인)
위원 신 현 우 (인)
위원 기 선 권 (인)

Abstract

Study on the protective effect of VISTA-positive kidney resident macrophages against renal injury

Jun-Gyu Park

Development of rodent model and advanced clinical research led to elucidate immunological mechanisms of kidney diseases. However, the profiling of resident immune-cell subsets especially macrophage in mouse and human kidneys remains undetermined. In order to understand immunological mechanism of kidney diseases, the renal resident immune cell composition and the role of macrophages in kidney should be further investigated. Resident macrophages have unique tissue-specific functions in maintaining tissue-homeostasis, resolving inflammation and regulating T cells. However, the repair mechanism and relevant molecules of kidney-resident macrophages after ischemic injury remain unresolved. In this study, resident immune-cell profiling was performed in mouse and human kidneys that were obtained from radically nephrectomised patients with urogenital malignancy. Furthermore, the function of kidney-resident macrophage, which plays an important role in maintaining kidney-homeostasis, regulating inflammation and T cells, was analyzed. As a result, in human kidneys, 47% ± 12% of immune cells were $CD3^+$ T cells. Kidney $CD4^+$ and $CD8^+$ T cells comprised 44% and 56% of total

T cells. Of these, 47% ± 15% of T cells displayed an effector memory phenotype ($CCR7^-CD45RA^-CD69^-$), and 48% ± 19% were resident memory phenotype ($CCR7^-$ $CD45RA^-$ $CD69^+$). The proportions of human kidney-resident macrophage were approximately 10% of total immune cells and had highest proportion in myeloid cells of the human kidney. In mouse kidneys, kidney-resident macrophages were the most predominant subset while the proportion of $CD3^+$ T cells was less than 20%. In both human and mouse, kidney-resident macrophages accounted for a high proportion in myeloid cells, and as a result of selectively depleting kidney-resident macrophages by treatment with clodronate liposomes in ischemia reperfusion injury model, recovery from renal injury was delayed. Moreover, V-domain Ig suppressor of T cell activation (VISTA), an immune checkpoint molecule, was constitutively expressed in mouse and human kidney-resident macrophages. By using VISTA knockout (KO) mice, it was confirmed that kidney-resident macrophages regulate elimination of dead cells and activation of T cells through VISTA, and that recovery from renal injury was delayed in VISTA KO mice. In conclusion, kidney-resident macrophages, the highest proportion in myeloid cells of human and mouse kidney, maintain kidney-homeostasis and repair from renal injury through tissue specific VISTA expression.

Keywords: kidney; inflammation; resident macrophage; T cell; Myeloid cell; VISTA.

Student Number : 2016—26385

TABLE OF CONTENTS

ABSTRACT

TABLE OF CONTENTS

LIST OF TABLES

LIST OF FIGURES

LIST OF ABBREVIATIONS

Ⅰ. INTRODUCTION · · · · · · · · · · · · · · · · · 1

Ⅱ. MATERIALS AND METHODS · · · · · · · · · 6

Ⅲ. RESULTS · 16

Immune-cell subsets in human kidneys · · · · · · · · 16

Immune-cell subsets in mouse kidneys · · · · · · · · 18

Two macrophage subsets within the kidney · · · · · · · 19

Repair from kidney inflammation depends on the resident macrophage · 22

VISTA expression in kidney macrophages · · · · · · · 23

Tissue environment affects VISTA expression · · · · · 25
Functional capacity of VISTA · · · · · · · · · · · · · · 28
VISTA^{+} macrophage in human kidney · · · · · · · · · 29

Ⅳ. DISCUSSION · 32

Ⅴ. REFERENCES · 82

Ⅵ. ABSTRACT IN KOREAN · · · · · · · · · · · · 88

LIST OF TABLES

Table 1. Baseline characteristics of human subjects for analysis of immune cell composition in human kidney..... 39
Table 2. Histological findings of human subjects for analysis of immune cell composition in human kidney..... 40
Table 3. Surface or intracellular markers of kidney R1, R2, and neutrophils 41
Table 4. Mean values and standard deviations of blood urea nitrogen and creatinine after ischemia–reperfusion injury.....42
Table 5. Baseline characteristics of human subjects for human macrophage analysis.....43
Table 6. Representative surface or intracellular markers of human kidney macrophage subsets 44

LIST OF FIGURES

Figure 1. Gating strategy for human T cell, B cell, and NK cell subsets in kidney 45
Figure 2. Lymphocytes and natural killer (NK) cells in human kidneys 46
Figure 3. Myeloid cells in human kidney 47
Figure 4. Lymphocytes and natural killer (NK) cells in mouse kidneys 48
Figure 5. Proportion of other immune cells in mouse kidney. 49
Figure 6. Myeloid cells in mouse kidneys 50
Figure 7. Two subtype of kidney macrophage.....51
Figure 8. Radiation resistance in R1 and R2 macrophages 52
Figure 9. The depletion kinetics of R1 macrophages by anti-CSF-1 receptor Abs or clodronate liposomes 53
Figure 10. Replacement rates of R1, R2 and Nϕ.....54
Figure 11. Development of kidney-resident macrophages.....55
Figure 12. Transcriptomic profiling of R1 and R2 56
Figure 13. IRI at bilateral kidney 57
Figure 14. Phagocytic activity of R1 and R2 macrophages 58
Figure 15. Proliferation capacity of kidney macrophages 59
Figure 16. Ischemic injury after depletion of kidney macrophages 60
Figure 17. Resolution of ischemic injury by kidney-resident

macrophage 61
Figure 18. R1-depleted mice showed tubular damage and harbored apoptotic cells 62
Figure 19. VISTA expression in kidney 63
Figure 20. The chromatin in the Vsir gene site was more accessibility in R1 macrophages than in R2 macrophages 64
Figure 21. VISTA expression in kidney-resident macrophages did not depend on various condition.....65
Figure 22. Expressions of immune checkpoint molecules in kidney 66
Figure 23. VISTA expression in tissue-resident macrophages...67
Figure 24. VISTA expression in tissue and R1 macrophages was remained elevated after ischemia reperfusion injury 68
Figure 25. Replacement of resident macrophages in the peripheral blood, spleen and peritoneum at 2 months after unilateral ischemia-reperfusion injury 69
Figure 26. VISTA expression of replaced and non-replaced kidney and peritoneal macrophages in the parabiosis model 70
Figure 27. Replacement rate of kidney macrophages after IRI 71
Figure 28. VISTA expression in bone marrow-derived macrophages with various condition 72
Figure 29. Tissue environment-dependent VISTA expression in kidney macrophages 73
Figure 30. *In vivo* or *In vitro* phagocytic capacity of VISTA.....74
Figure 31. VISTA inhibited the activation and proliferation of naïve

T cells and their IFN−γ secretion.....75
Figure 32. Baseline number of kidney T cells in Vsir$^{-/-}$ mice 76
Figure 33. Loss of VISTA delayed the repair from the induction of ischemia−reperfusion injury(IRI).....77
Figure 34. Loss of VISTA inappropriately regulated T cell activation and proliferation after IRI.....78
Figure 35. The characterization of human macrophages including kidney−resident macrophage.....79
Figure 36. VISTA expression in human kidney macrophage and T cells.....80
Figure 37. VISTA inhibited the proliferation of human T cells.....81

LIST OF ABBREVIATIONS

VISTA	V-domain immunoglobulin suppressor of T cell activation
VSIG3	V-set and Ig domain-containing protein 3
PSGL-1	P-selectin glycoprotein ligand-1
MerTK	MER Proto-Oncogene, Tyrosine Kinase
Tim4	T-cell immunoglobulin- and mucin-domain-containing 4
GVHD	Graft-versus-Host disease
EAE	Experimental Autoimmune Encephalomyelitis
MHC	Major histocompatibility complex
HLA	Human leukocyte antigen
IRI	Ischemia reperfusion injury
CL	Clodronate liposome
PL	PBS liposome
ATAC-seq	Assay for Transposase-Accessible Chromatin using sequencing
TUNEL	Terminal deoxynucleotidyl transferase dUTP nick end labeling
Nϕ	Neutrophil
rMac	Resident macrophages
iMac	Infiltrating macrophages
Large PM	Large peritoneal macrophage
Small PM	Small peritoneal macrophage

PM	peritoneal macrophage
cPM	In vitro cultured peritoneal macrophage
Alv Mac	Alveolar macrophage
Int Mac	Intestinal macrophage
SRPM	Splenic red pulp macrophage
Sup	Supernatant
M-CSF	Macrophage colony-stimulating factor
LPS	Lipopolysaccharide
TGF-β	Transforming growth factor-β
IFN	Interferon
TNF-α	Tumor necrosis factor-α
IL	Interleukin
LIF	Leukemia inhibitory factor
PMA	Phorbol 12-myristate 13-acetate
Poly I:C	Polyinosinic-polycytidylic acid
BMDM	Bone marrow derived macrophage
CFSE	Carboxyfluorescein succinimidyl ester
T_E	Effector T
T_{EM}	Effector memory T
T_{CM}	Central memory T
T_{reg}	Regulatory T
T_{EMRA}	CCR7$^-$CD45RA$^+$ T
T_{RM}	Tissue-resident memory T
cDCs	Classical Dendritic cells
BUN	Blood urea nitrogen

PBMC	Peripheral blood mononuclear cell
Abs	Antibodies
SEM	Standard error of the mean

Ⅰ. INTRODUCTION

Understanding immune dysregulation in kidney diseases has been advanced recently because of sophisticated mouse studies and clinical studies.[1] Chronic kidney disease, acute kidney injury, end-stage renal disease, or even genetic disorders are directly or indirectly immune-mediated,[2,3] and thus several immune-modulating agents have been investigated in clinical trials.[4] Current options are restricted to conventional systemic agents such as glucocorticoids, calcineurin inhibitors, and mycophenolic acid or non-immune-modulating agents, including angiotensin converting enzyme inhibitor and angiotensin II receptor blocker.[5,6] Targeting agents such as Rituximab and Belatacept have been used in certain kidney diseases such as lupus nephritis, vasculitis, and kidney transplantation.[7,8] Despite the efficacy of these agents, further immune-cell-targeting agents are needed to improve patient outcomes and decrease systemic side effects. To accomplish this, investigation of the renal immune system should be accomplished in mice and human. Kidney injury triggers inflammation and subsequent repair processes. Although the detailed mechanism underlying the repair response remains partly unclear, studies have shown that several subpopulations of immune cells infiltrate into the kidneys and may determine the degree of injury or recovery.[9]

Recent studies revealed that certain resident immune cells, especially macrophages, are predominant in human peripheral tissues

such as the brain and lungs,[10,11] but information on resident immune cells in human kidneys is lacking.[12] Analysis of resident immune-cell subsets in mice and human kidneys may enhance understanding of homeostasis, inflammation, and disease.

Tissue-resident immune cells, particularly macrophages, have been reported to have a role in tissue homeostasis and protecting against inflammatory processes including infection, allergic reactions and cancer.[13-15] Even in non-inflammatory conditions, these cells maintain tissue-homeostasis,[16,17] and non-immune parenchymal cells or the infiltrating immune cells alone may not be sufficient for maintaining tissue-homeostasis. The functions of tissue-resident macrophages are closely associated with the tissue micro-environment in which they reside and changes following stimuli.[18,19] However, what happens inside the tissue milieu and the cell interactions with tissue components have been poorly explored from the standpoint of kidney-resident macrophages. The presence of tissue-resident macrophages is determined by selective lineage markers and gene mapping assays.[20,21] These cells can maintain themselves in adulthood through self-renewal independently of blood monocytes,[22] which suggests they have roles independent of monocyte-derived tissue-infiltrating macrophages. Kidney-resident macrophages monitor and scavenge the endothelial transport of immune complexes and subsequently trigger type III hypersensitivity.[23] These phenomena are crucial in diseases attributable to insufficient clearance of immune complexes, such as

systemic lupus erythematosus.[24] The proangiogenic activity of kidney-resident macrophages is also up-regulated during renal artery stenosis.[25] Nevertheless, the roles of kidney-resident macrophages both in homeostasis and pathologic conditions are still poorly understood. Few studies have examined the gene signatures in kidney-resident macrophages, limiting the understanding of their biological functions.[20]

Immune checkpoints are critical therapeutic targets in various diseases such as cancer, autoimmune diseases and other inflammation.[26,27] Co-inhibitory immune checkpoints are up-regulated or induced in antigen-presenting cells upon interaction with T cells whose activation needs to be regulated.[28]

V-domain immunoglobulin suppressor of T cell activation (VISTA) is one of the immune checkpoint molecules. VISTA expressed on T cells and myeloid cells.[29] VISTA can function as an inhibitory ligand on antigen-presenting cells (APCs) and regulate T cell responses through binding partner that was proposed V-set and Ig domain-containing protein 3 (VSIG3) and P-selectin glycoprotein ligand-1 (PSGL-1).[30,31] VSIG3 can mediate functional inhibition of human T cell activation.[30] Binding of PSGL-1 to VISTA at lower pH around 6.5 suggested possible engagement of VISTA in acidic environments such as tumor microenvironment and this was confirmed by the acidic pH-selective antibody.[31] Previous study demonstrated role for VISTA as a negative checkpoint regulator in tumor immunity. 13F3, a VISTA-specific monoclonal antibody was

identified to neutralize VISTA, was shown to suppress growth of CT26 colon cancer, B16OVA melanoma, MB49 bladder carcinoma, B16BL6 melanoma.[32,33] Also, VISTA affects various immune diseases such as Graft-versus-Host disease (GVHD), Hepatitis, Lupus, Experimental Autoimmune Encephalomyelitis (EAE).[29,34] Recent study has proven that VISTA plays a role in maintaining the quiescent state of $CD4^+$ cells.[35]

I investigated resident immune-cell composition of normal kidney and whether kidney-tissue resident macrophages regulate tissue repair and T cell regulation in homeostasis and ischemic renal injury. In human kidneys, 47% of immune cells were $CD3^+$ T cells. Of these, 48% of $CD3^+$ T cells displayed a resident memory phenotype. The proportion of human kidney-resident myeloid cells was 10% of immune cells. Of these, macrophages occupied most of myeloid cells. In mouse kidneys, kidney-resident macrophages were the most predominant subset. Since myeloid cell subsets in both human and mouse kidneys were comprised of tissue-resident macrophages, which is known to play an essential role in tissue homeostasis and regulation of T cells, I conducted further research on this immune-cell subset. As a results, tissue repair from renal inflammation depends on kidney-resident macrophages. Unexpectedly, all mice and human kidney-resident macrophages expressed VISTA, even during homeostasis, whereas other tissue-resident macrophages had different expression patterns, which indicate tissue-specific characteristics. VISTA helped kidney-resident macrophages to

accelerate repair after ischemic renal injury. The present study confirmed the existence of resident immune-cells in kidney, and revealed that especially tissue-resident macrophages protect against renal injury through VISTA.

Ⅱ. MATERIALS AND METHODS

Mice

C57BL/6(B6), B6.CD45.1, NSG, B6.*Rag1*$^{-/-}$, *LysM*-Cre, *Rosa26*-*mTmG*, and BALB/c wild type mice were purchased from the Jackson Laboratory (ME, USA). B6.*Vsir*$^{-/-}$ mice were established and bred using a cryopreserved sperm (KOMP Repository, UC Davis, CA, USA). B6.CD1d$^{-/-}$ and B6.Jα18$^{-/-}$ mice were provided by Masaru Taniguchi (RIKEN Center for Integrative Medical Sciences, Japan). B6.*MyD88*$^{-/-}$ mice were provided by Professor Jaeseok Yang (Seoul National University College of Medicine). db/db mice were purchased from the SLC Inc. (Japan). *LysM-Cre* mice were interbred with *Rosa26-mTmG* mice to generate *LysM-Cre-Rosa26-mTmG* mice. Unless stated otherwise, all mice used in experiments were 8 weeks of age. Animals were housed under specific pathogen-free conditions at the Seoul National University College of Medicine. All experiments were approved by the Seoul National University Institutional Animal Care and Use Committee (no. SNU-150611-1-19) and in accordance with the guidelines.

Characterization of murine and human immune cells

Kidney tissue was minced and digested with 40 μg/mL DNase Ⅰ and 1 mg/mL collagenase D for 30—45 min at 37℃. Cells were filtered through a 40—μm strainer, suspended in 40% Percoll underlain with 80% Percoll (GE Healthcare Life Sciences, Buckinghamshire, UK)

and centrifuged. The middle layer, an enriched population of leukocytes, was harvested. Peritoneal immune cells were obtained using the peritoneal injection of 5 mL of cold PBS. The study design for human samples was approved by the institutional review board of the Seoul National University Hospital (no. H-1810-016-975) and complied with the Declaration of Helsinki. All patients provided written informed consent for the donation and use of their specimens.

Flow cytometry

Cells were washed, resuspended in staining buffer consisting of 2% horse serum and 0.05% sodium azide, blocked with anti-mouse CD16/CD32 Abs (clone 2.4G2) or anti-human Fc receptor binding inhibitor (eBioscience, CA, USA) for 10 min at 4℃, and then incubated with primary Abs. Alternatively, following surface staining, cells were incubated with fixation-permeabilization buffer, washed with permeabilization buffer (Fixation/Permeabilization Solution Kit; BD Biosciences, CA, USA), and then incubated with Abs against intracellular antigens. Samples were processed by a BD Fortessa™ (BD Biosciences). Cell sorting was performed by a BD FACSAria III (BD Biosciences). All FACS results were analyzed with FlowJo software (FlowJo, LLC, OR, USA).

Cell morphology

Sorted cells were spun at 800 rpm for 10 min in a cytocentrifuge (Cytopro 720; Wescor Inc., UT, USA). Cytospin slides were fixed

with methanol and air dried. Slides were then stained with Giemsa (Sigma-Aldrich, MO, USA).

Induction of ischemia reperfusion injury

Mice were anesthetized with ketamine (100 mg/kg of body weight) and xylazine (10 mg/kg of body weight). After bilateral flank incisions, both renal pedicles were cross-clamped for 30 min with microaneurysm clamps (Fine Science Tools, Inc., CA, USA). During the procedure, animals were placed on a heating pad (37℃). Prewarmed PBS (200 μL) was administered subcutaneously for optimal fluid balance. The mice were sacrificed at the indicated time points after reperfusion. Sham-operated mice underwent the same surgical procedure except for the clamping of the renal pedicles. In the parabiotic set, clamping in a unilateral side of each parabiont was performed. Renal function was evaluated by blood urea nitrogen and serum creatinine levels using an autoanalyzer (Hitachi Chemical Industries, Ltd., Japan).

Generation of parabiotic mice

B6 8-week-old CD45.1 and CD45.2 congenic mice were surgically connected as previously described.[9] After the corresponding lateral skin incisions were made from the elbow to the knee in each mouse, fore-limbs and hind-limbs were tied together using nylon suture, and the skin incisions were closed using stainless steel wound clips.

After surgery, mice were maintained on a diet supplemented with trimethoprim/sulfamethoxazole for prophylaxis of infection.

Transcriptomics analysis of kidney immune cells

The Affymetrix Whole-transcript Expression array was performed according to the manufacturer's protocol (GeneChip WT Pico reagent kit: Thermo Fisher Scientific, CA, USA). cDNA was synthesized using the GeneChip WT Pico amplification kit (Thermo Fisher Scientific). The cDNA was then fragmented and biotin-labeled with terminal deoxynucleotidyl transferase using the GeneChip WT terminal labeling kit (Thermo Fisher Scientific). Approximately 5.5 μg of labeled cDNA was hybridized to the Affymetrix GeneChip mouse gene 2.0 ST array at 45℃ for 16 h. Hybridized arrays were washed and stained by a GeneChip Fluidics Station 450 and scanned by a GCS3000 Scanner (Thermo Fisher Scientific). Signal values were computed using the Affymetrix GeneChip™ Command Console software (Thermo Fisher Scientific).

Gene expression analysis by real-time RT-PCR

RNA was purified from 2×10^6 sorted cells (5 mice) using a Direct-zol™ RNA MicroPrep kit (Zymo Research, CA, USA). RNA was reverse transcribed to cDNA with a PrimeScript™ RT reagent kit (TaKaRa Bio Inc., Otsu, Shiga, Japan). Gene expression was evaluated by real-time RT-PCR using an iQ™ SYBR® Green Supermix (Bio-Rad, CA, USA) on a PCR amplification and detection

instrument (CFX Connect Real-Time PCR Detection System; Bio-Rad). Primer sequences were as follows: *Vsir*, forward 5'-AAACCACCACCCAGAACAA-3' and reverse 5'-GTCACTGTCCT-GCTCATTAGAC-3'; and *Actb*, forward 5'-CGCCACCAGTTCGCC-ATGGA-3' and reverse 5'-TACAGCCCGGGGAGCATCGT-3'. Gene expression was normalized to β-actin, and the mean relative gene expression was calculated using the $2^{-\Delta\Delta C(t)}$ method.

Assay for Transposase-Accessible Chromatin (ATAC) sequencing

Nuclei harvested from R1 and R2 macrophages were subjected to the transposition reaction with Tn5 transposase (Illumina, CA, USA) in tagmentation DNA buffer, and library fragments were amplified with indexing primers from the Nextera kit (Illumina).[13] The multiplexed libraries were sequenced on the Illumina NextSeq 500 for single read 75 bases and analyzed using bcl2fastq2 v2.15 base calling software and ASCII Qscore Offset 33. Fastq files were aligned to mm10 using Bowtie2 and used for peak calling with Homer software. Peak enrichment files in Homer were converted to bigWig files for viewing the data in the UCSC Genome Browser (https://genome.ucsc.edu). Peak enrichment regions that fell below the false discovery rate (FDR < 0.05) and within 100 kb of the transcription start site or the transcription end site were considered for further analysis. These analysis were performed by Professor Hyun Mu Shin (Seoul National University College of Medicine).

In vivo and *ex vivo* phagocytosis assay

For the *in vivo* assay, 2×10^7 fluorescence-labelled apoptotic thymocytes, which were induced with 0.1 μM dexamethasone in 10^7 cells/mL of complete DMEM for 15 h at 37℃, or 0.5 mg/mL pHrodo Green *E. coli* Bioparticle (Thermo Fisher Scientific) were administered via the tail vein. At the indicated time, mice were euthanized, and their kidneys and lungs were harvested for flow cytometry. In experiments with *LysM-Cre-Rosa26-mTmG* mice, the expression of tdTomato was calculated using mean fluorescence intensity in $EGFP^+$ macrophages.

For the *ex vivo* assay, 2×10^5 kidney cells were incubated in Opti-MEM with 8×10^5 fluorescence-labelled apoptotic thymocytes for 2 h at 37℃. In another experiment, 5×10^5 kidney cells were incubated in Opti-MEM with 0.5 mg/mL pHrodo Green *E. coli* Bioparticle (Thermo Fisher Scientific) for 2 h at 37℃. At the indicated time, cells were analyzed by flow cytometry.

In vivo depletion of macrophages

For macrophage depletion, clodronate liposomes (CLs) or PBS liposomes (PLs) (100 μL per 10 g of body weight) were administered via the tail vein. In another experiment, mice were treated with anti-CSF-1 receptor Abs (clone BE0213; Bio X Cell, NH, USA) for 4 days as follows: low dose setting, 1 mg at day 0 and then 0.3 mg from day 1 to day 3; or high dose setting, 1 mg from day 0 to day 3. For irradiation, mice were placed in an acrylic container and treated with

a single dose of 2.5, 5.5 or 9.5 Gy from a source of ^{137}Cs (Cisbio International, Bagnols-sur-Cèze, France).

Kidney histology

Kidneys were fixed in 4% formalin, paraffin embedded and cut into 4—μm sections. Sections were then stained with periodic acid-Schiff before microscopy analysis (Leica Microsystems, Wetzlar, Germany). The assessment of tubular injury in the cortex was graded in a blinded manner based on the percentage of tubular dilatation, cast deposition, brush border loss, and necrosis as follows: 0, no involvement; 1, < 10% involvement; 2, 10%—25% involvement; 3, 25%—50% involvement; 4, 50%—75% involvement; and 5, > 75% involvement. Ten random fields per kidney section (200× magnification) were used for quantification. Apoptotic cells were identified in tissue sections by terminal deoxynucleotidyl transferase dUTP nick end labeling (TUNEL) using the Click-iT TUNEL imaging assay (Thermo Fisher Scientific) according to the manufacturer's instruction.

Western blotting

Equal amounts (10 μg) of extracted protein were separated on 10% SDS-polyacrylamide gels and transferred onto Immobilon-FL 0.4 μM polyvinylidene difluoride membranes. After blocking, membranes were probed with primary Abs. The blots were developed and enhanced using a SuperSignal West Femto Maximum Sensitivity

Substrate kit (Thermo Fisher Scientific). Band intensity was assessed by ImageJ software (version 1.5; National Institutes of Health, MD, USA).

Culture of BMDMs and peritoneal macrophages

To prepare bone marrow-derived macrophages (BMDMs), bone marrow cells (2×10^6) from wild-type B6 mice were grown in DMEM containing 10% fetal bovine serum (FBS), antibiotic-antimycotic and 10% L929 cell supernatant (mouse fibroblasts; Korean Cell Line Bank, Seuol, Korea) or the indicated concentration of recombinant mouse macrophage colony-stimulating factor (M-CSF) (R&D Systems, MN, USA). L929 cells were maintained in DMEM supplemented with 10% FBS and 10 U/mL penicillin. After 7 days, BMDM cells were harvested and treated with the indicated concentration of cytokines or stimulants.

For peritoneal macrophages, cells from peritoneal fluids were incubated in the above DMEM for 2 h, followed by washing with PBS to remove non-adherent cells. Remnant adherent cells were cultured for 3 days and harvested for subsequent experiments.

T cell proliferation assay

$CD62L^+$ $CD4^+$ or $CD62L^+$ $CD8^+$ T cells from lymph nodes were labeled with CFSE and cultured in 96-well flat-bottom plates coated with anti-mouse CD3 Abs (clone 2C11) and VISTA-Fc or control-Fc (R&D Systems) at the indicated concentration. For human T cells,

$CD4^+$ or $CD8^+$ T cells from peripheral blood mononuclear cells were labeled with CFSE and stimulated with anti-human CD3 Abs (clone OKT3) and VISTA-Fc or control-Fc (R&D Systems) at the indicated concentration. After the indicated times, cells were harvested and analyzed by flow cytometry.

IFN-γ production

Quantification of IFN-γ release in cell supernatants of *in vitro* T-cell culture was performed by enzyme-linked immunosorbent assay using capture and detection Abs.

In vivo macrophage proliferation

Mice were intraperitoneally treated with 10 mg/kg 5-ethynyl-2-deoxyuridine (EdU) for 3 days. Then, IRI was induced. Kidneys were harvested at the indicated time, and proliferation was determined with the Click-iT EdU assay (Thermo Fisher Scientific) according to the manufacturer's instruction.

Statistical analysis

All analyses and calculations were performed using GraphPad Prism (version 7.0; GraphPad Software, Inc., CA, USA). The results are expressed as mean ± standard error of the mean (SEM). Differences between groups were evaluated using the Student's *t*-test. Survival curves were drawn using the Kaplan-Meier method. To compare

survival curves between groups, the log-rank test was applied. $P < 0.05$ was considered statistically significant.

Ⅲ. RESULTS

Immune-cell subsets in human kidneys

First, I explored resident immune cell subsets in human kidneys to investigate renal immune system. Fifteen kidney tissues from radical nephrectomy cases were analyzed by flow cytometry. The mean age of patients was 69 ± 10 years. Ten patients (66.7%) were male. The mean values of serum creatinine and the estimated glomerular filtration rate calculated by the Chronic Kidney Disease Epidemiology Collaboration equation[36] were 1.0 ± 0.3 mg/dL and 73.6 ± 15.2 mL/min/1.73 m^2, respectively. Thirteen patients (86.7%) had estimated glomerular filtration rates greater than 60 mL/min/1.73 m^2. Three patients (20%) had proteinuria by dipstick test, and all the levels were 1+. Other baseline characteristics are shown in Table 1. Histologic findings are shown in Table 2. Flow cytometric analysis of immune- cell subsets in kidney tissues from patients who underwent radical nephrectomy was performed. Figure 1 shows the representative gating strategy for T cell, B cell, and natural killer cell subsets. The proportion of $CD3^+$ T cells was 47.4% ± 11.6%, of which approximately 44% and 56% were $CD4^+$ and $CD8^+$ T cells, respectively.

Among $CD4^+$ T cells (Figure 2A), the main subsets were $CCR7^-$ $CD45RA^-$ cells (effector memory; T_{EM}: 44.5% [9.3% of $CD45^+$ cells]) and $CD69^+$ cells (tissue-resident memory; T_{RM}: 39.3% [8.2% of $CD45^+$ cells]). Among $CD8^+$ T cells (Figure 2B), the main subsets

were T_{EM} (24.3% [6.4% of $CD45^+$ cells]), T_{RM} (57.9% [15.3% of $CD45^+$ cells]), and $CCR7^-$ $CD45RA^+$ cells (T_{EMRA}) (20.7% [5.5% of $CD45^+$ cells]). When I grouped T_{RM} cells by the expression of CD103 and CD49a,[37] $CD49a^-$ $CD103^-$ and $CD49a^+$ $CD103^-$ T_{RM} cells were the predominant subsets in $CD4^+$ T_{RM} cells, and $CD49a^-$ $CD103^-$, $CD49a^+$ $CD103^-$, and $CD49a^+$ $CD103^+$ T_{RM} subsets were predominant in $CD8^+$ T_{RM} cells. However, $CD49a^-$ $CD103^+$ T_{RM} cells were the minor subset in $CD4^+$ and $CD8^+$ T_{RM} cells (< 1% of $CD45^+$ cells). Regarding other T cell subsets, regulatory T (Treg), gamma/delta (γδ) T, and $CD56^+$ T cells were less than 10% of $CD45^+$ immune cells (Figure 2C). The proportions of NK and B cells were 18.2% ± 10.5% and 1.4% ± 1.2%, respectively (Figure 2D). Among NK cells, the $CD56^{dim}$ subset was the main population. Class-switched memory B cells and plasma cells constituted less than 1% of $CD45^+$ cells. The gating strategy for myeloid cells including macrophages, classical dendritic cells (cDCs), and neutrophils is shown in Figure 3A. The proportion of the $CD14^+$ macrophages subset was 10.2% ± 4.7%. Most $CD14^+$ macrophages subsets in the kidney did not express CD16, and thus, these were categorized by the expression levels of CD64 and HLA-DR.[38] Among $CD14^+$ cells, $CD64^+$ $HLA-DR^+$ (35.1% [3.6% of $CD45^+$ cells]) and $CD64^+$ $HLA-DR^-$ cells (53.6% [5.4% of $CD45^+$ cells]) were the main subsets, and $CD64^-$ $HLA-DR^-$ cells were the minor subset (11.3% [1.2% of $CD45^+$ cells]) (Figure 3B). There were almost no $CD64^-$ $HLA-DR^+$ cells among $CD14^+$ cells. The proportions of cDCs and neutrophils were 1.1% ± 0.6% and 11.5% ± 5.8%, respectively.

Collectively, the most abundant resident myeloid cell subset was $CD14^+$ macrophages and T_{RM} was most abundant subset of T cells in human kidney.

Immune-cell subsets in mouse kidneys

Next I analyzed resident immune-cell subsets in mouse kidney. Because human samples were obtained from older patients, 1-year-old mice were analyzed in addition to 8-week-old mice. Harvested kidneys from 8-week- and 1-year-old B6 mice were evaluated after perfusion with 10 mL of cold PBS via the left chamber of the heart. Figures 4A and 4B show the representative gating strategy for T cells and their proportions. Total $CD3^+$ T cells accounted for 11.4% ± 2.1% and 14.2% ± 1.3% in 8-week- and 1-year-old mice, respectively. Among the $CD3^+$ T cells in 8-week-old mice, $CD4^+$ and $CD8^+$ T cells accounted for 60% and 40%, respectively. For 1-year-old mice, $CD4^+$ and $CD8^+$ T cells accounted for 55% and 45%, respectively. The most abundant T cell subset was $CD62L^-CD44^-$ cells in 8-week-old mice, whereas $CD62L^-CD44^+$ cells were most abundant in 1-year-old mice (Figure 4B). The T_{RM} subset was less than 0.5% of $CD45^+$ immune cells. Regarding other T cell subsets, Treg, γδT, and natural killer T (NKT) cells were less than 1% of $CD45^+$ immune cells, except in 1-year-old mice where 5% of cells were NKT cells (Figure 5A). The proportions of NK and B cells were 7.8% ± 1.1% and 21.4% ± 0.7%, respectively, in 8-week-old mice,

and 6.5% ± 0.7% and 17.9% ± 5.2% in 1-year-old mice (Figure 5B).

The gating strategy and proportions of macrophages, monocytes, DCs, and neutrophils are shown in Figure 6A and 6B. The proportions of macrophages were 45.4% ± 4.0% and 39.2% ± 4.0% in 8-week- and 1-year-old mice, respectively. When macrophages were categorized into kidney-resident (rMac: $CD11b^{low}$ $F4/80^{high}$) and kidney-infiltrating (iMac: $CD11b^{high}$ $F4/80^{low}$) subsets,[39] more than 90% were rMac (Figure 6B). Other myeloid subsets such as neutrophils and dendritic cells were less than 1% of $CD45^{+}$ cells. Collectively, macrophages were the most abundant immune cell subset in the mouse kidney.

Two macrophage subsets within the kidney

Previous results indicate that the human kidney predominantly harbors T cells, especially effector memory and resident memory cell subsets while mouse kidney predominantly harbors resident macrophages. However, in both mouse and human, kidney-resident macrophages accounted for a high proportion in myeloid cells. And it is known that tissue-resident macrophages play an essential role in tissue homeostasis. Moreover, not only in presenting foreign antigen to T cells, macrophages also have a pivotal role in providing required co-stimulatory molecules and cytokines that ensure effective T cell activation.[40] Based on these previous research, I hypothesized that tissue-resident macrophage plays a key role during regulation of T

cell in tissue environment. Thus, I proceeded to research on kidney-resident macrophages and their role in homeostatic status and renal injury.

Kidney macrophages are classified by CD11b and F4/80 expressions:[23,41] $CD45^+$ $Ly6G^-$ $CD11b^{int}$ $F4/80^{high}$ (resident subset; herein, termed R1) and $CD45^+$ $Ly6G^-$ $CD11b^{high}$ $F4/80^{int}$ macrophages (infiltrating subset; herein, termed R2) (Figure 7A). $CD45^+$ $Ly6G^+$ cells are neutrophils. R1 macrophage numbers were higher than R2 macrophages in kidneys of wild-type adult mice (Figure 7A). The cytoplasm and cell size of R1 macrophages were smaller than those of R2 macrophages (Figure 7B). Both R1 and R2 macrophages expressed CD11c and MHC class II (Table 3 and Figure 7C), indicating they share markers of dendritic cells within kidney tissues.[42] However, the expression level of MHC class II was higher in R1 macrophages than in R2 macrophages, and R1 macrophages did not express Ly6C. Other surface and intracellular markers of R1 and R2 macrophages are summarized in Table 3.

Several different characteristics were observed between R1 and R2 macrophages. The radio-sensitivity of R1 macrophages was lower than that of R2 macrophages (Figure 8), but the depletion kinetics of R1 macrophages by anti-CSF-1 receptor Abs or clodronate liposomes (CLs) were extended compared with that of R2 macrophages (Figure 9A and 9B), possibly because of the different source of each macrophage subset. To address the origin of macrophages, the parabiosis model using CD45 congenic mice was

applied. The tissue-residency of R1 macrophages was confirmed, and R2 macrophages were continuously stuffed by monocyte-derived macrophages (Figure 10A—C). Normal development of R1 and R2 macrophages was observed in female mice, BALB/c mice, and several knockout (e.g., CD1d$^{-/-}$, Jα18$^{-/-}$, NOD/SCID-gamma null [NSG], *Rag1*$^{-/-}$) or mutation strains (e.g., db/db), particularly in *MyD88*$^{-/-}$ mice and innate T or adaptive T or B cell-deficient mice (Figure 11).

Transcriptomic profiling of R1 and R2 macrophages was performed (Figures 12A—E). A total of 986 genes were differentially expressed by at least two-fold between the two subsets. *Mertk*, *Axl*, *Tgfbr1* and *Mmp12*/*Mmp13* were highly expressed in R1 macrophages, and *S100a4*, *S100a6*, *Ceacam1* and *Ccr2* were highly expressed in R2 macrophages (Figure 12A). Scatter and volcano plots also demonstrated the differences between the two macrophage subsets (Figure 12B and 12C). The gene expression in R1 macrophages also differed from that of peritoneal macrophages with or without *in vitro* culture (Figure 12A and 12D). Gene set enrichment analysis showed that differentially expressed genes in R1 macrophages were primarily associated with positive or negative regulation of other immune cells (Figure 12E). However, differentially expressed genes in R2 macrophages were associated with the inflammatory response and cell adhesion. These results suggest that the functional capacity may differ between these two

subsets during homeostasis or the initial inflammatory process, such as regulation in R1 and inflammation in R2 macrophages.

Repair from kidney inflammation depends on the resident macrophage

I induced bilateral ischemia reperfusion injury (IRI) model to the mouse to determine the role of kidney-resident macrophage during renal injury. IRI at bilateral kidneys was performed and repair was identified after 72 h (Figure 13A). In the absence of pre-conditioning, the number of R2 subset cells increased, while the number of R1 subset cells was unchanged following IRI (Figure 13B). These results support previous studies reporting different cellular kinetics between macrophage subsets following IRI.[43,44] Both R1 and R2 macrophages participated in phagocytosis following IRI (Figure 14A), and their phagocytic activity was higher after IRI (Figure 14B). The proliferation capacity was higher in R2 macrophages than in R1 macrophages following IRI (Figure 15A and 15B). When total macrophages were depleted, the overall ischemic damage was abrogated (Figure 16A), which is consistent with previous data.[45] Notably, the depletion time point (early *vs.* late) for macrophages may result in different outcomes.[42] I hypothesized that depleting one macrophage subset is needed to fully understand the above results and to elucidate the function of each subset during inflammation and repair processes. To this end, I used R1 macrophage characteristics,

such as their slow replacement rate compared with R2 macrophages following depletion.[21] In kidney macrophages depleted by CL, the depletion and repletion kinetics differed between R1 and R2 macrophages (Figure 9B). R1 macrophages were absent in CL-treated mice for 2 weeks and then slowly returned (Figure 16B). I thus used this time point (2 weeks after CL treatment) in which the kidney harbored mainly R2 macrophages but not R1 macrophages, for IRI. CL-treated mice (i.e., deficiency in R1 subset cells) revealed high levels of injury markers such as blood urea nitrogen and creatinine compared with PL-treated control mice at 72 and 96 h after IRI, which represented delayed repair from injury in the R1-depleted mice (Figure 17A and Table 4). At 48 h after IRI, the number of infiltrated R2 macrophages was higher in CL-treated mice than that in the PL-treated mice (Figures 17B and 17C). However, the overall cell number of R2 was not different between the two groups at 72 and 96 h, which indicated that depleted R1 macrophages, but not the infiltrated R2 subset, primarily participated in repair. At 96 h, R1-depleted mice still showed tubular damage, such as tubular dilatation and casts (Figure 18A), and harbored higher numbers of $TUNEL^+$ apoptotic cells than R1-intact mice (Figure 18B). These results indicate that tissue repair from renal inflammation depends on kidney-resident macrophages.

VISTA expression in kidney macrophages

I further researched on the molecules related to the repair function of kidney-resident macrophages. Among several different genes between R1 and R2 macrophages, the transcription of *Vsir*, which encodes the VISTA (an inhibitory immune checkpoint molecule), was up-regulated in R1 macrophages (red arrow in Figure 12A; and Figure 19A). This observation was interesting because VISTA was an inducible, not constitutively expressed, molecule in previous studies of inflammatory or cancerous conditions.[29,46] I hypothesized that persistent expression of VISTA on kidney-resident macrophages will continuously regulate the immune response during homeostatic status and kidney inflammation.

In kidney-resident immune cells, VISTA expression was dominant in $CD45^+$ $CD11b^+$ myeloid cells compared with $CD45^-$ or $CD45^+$ $CD3^+$ T cells or their subsets such as $CD4^+$, $CD8^+$, and double-negative T cells. VISTA expression was higher in R1 macrophages than in R2 macrophages but undetectable in neutrophils (Figure 19B—D).

To investigate the regulation of *Vsir*, I examined chromatin accessibility of the *Vsir* gene in R1 and R2 macrophages using ATAC sequencing. The degree of chromatin accessibility (termed openness) was numerated only near the transcription start sites and 5′ untranslated region as proximal regulatory regions reflecting gene expression. Between the two macrophage subsets, 8,790 proximal regulatory regions differed: 8,625 regions in R1 macrophages and 165 regions in R2 macrophages. Integration of ATAC sequencing

data with the microarray data showed that 227 regions were open in R1 macrophages and associated with increased gene expression (blue dots); 196 regions were open and associated with decreased gene expression in R1 macrophages (green dots); and 81 regions were open in R2 macrophages and associated with increased gene expression (red dots) (Figure 20A). The volcano plot for this data is shown in Figure 20B. The chromatin in the *Vsir* gene site was open in both R1 and R2 macrophages; however, the openness of two regions, *Vsir-2* and *Vsir-3*, was higher in R1 macrophages than in R2 macrophages (Figure 20C).

VISTA expression in R1 macrophages remained elevated irrespective of aging, strain and location (i.e., cortex or medulla) (Figure 21A—C). However, other immune checkpoint molecules, such as PD-L1, PD-L2, and galectin-9, were not expressed in R1 and R2 macrophages, with the exception of some R2 cells expressing PD-L1 (Figure 22A). Kidney-resident $CD4^+$ and $CD8^+$ T cells did not express inhibitory immune checkpoint molecules (Figure 22B). To be summarized, kidney R1 (and some R2) macrophages constitutively expressed VISTA even in non-injured kidneys, which was different from other immune checkpoint molecules and previous ideas that VISTA is induced in inflammation or the tumor microenvironment.[47]

Tissue environment affects VISTA expression

The expression patterns of MER Proto-Oncogene, Tyrosine Kinase (MerTK) and T-cell immunoglobulin- and mucin-domain-containing molecule (Tim4) in macrophages are dependent on the tissue specificity.[20] I hypothesized that VISTA expression in resident macrophages is dependent on the tissue-environment. VISTA levels were high in kidney, peritoneum, spleen and BM, but low in the liver, brain, lung and skin (Figure 23). After IRI, the overall tissue expression of VISTA was not altered (Figure 24A) and VISTA expression in R1 macrophages remained elevated (Figure 24B). To further dissect the effect of the tissue environment on VISTA, I used a congenic parabiosis model, in which the replacement rates of peripheral blood, spleen and peritoneal cells by paired parabiont cells were > 30% within 2 months (Figure 25). The replacement rate of R1 macrophages by paired parabiont macrophages was less than 3% within 2 months, whereas the replacement rate of R2 macrophages was approximately 30% (Figure 10). The VISTA expressions of R1, R2, and peritoneal (large and small) macrophages were similar between self and paired parabiont cells (Figure 26A). The replaced cells and non-replaced cells showed similar levels of activation markers, such as CD80, CD86 and MHC class II (Figure 26B). I next established parabiosis in mice and induced IRI in a unilateral kidney after 14 days to examine VISTA levels in replaced macrophages in inflammatory condition. The 14—day timeframe was chosen because no replacement of R1 macrophages by paired parabiont cells occurred until that time (Figure 10). The replacement rate of R1 macrophages

by paired parabiont cells in IRI-treated kidneys was higher than that in non-injured kidneys (Figure 27A), suggesting that inflammatory conditions enhance the replacement of resident macrophages by infiltrating monocyte-derived macrophages. The replaced R1 and R2 macrophages expressed VISTA at a similar level to the corresponding non-replaced macrophages (Figure 27B).

Interestingly, whereas isolated BM macrophages expressed VISTA (Figure 23), BMDMs, in which *in vitro* cultured cells were confirmed as $CD11b^{+}$ $F4/80^{+}$ macrophages, lost VISTA expression (Figure 28A). VISTA expression in BMDMs did not recover even in the presence of various cytokines or stimulants, such as CpG, lipopolysaccharide, transforming growth factor-β, tumor necrosis factor (TNF) -α, interferon (IFN) -β, IFN-γ, interleukin (IL)-4, IL-6, phorbol myristate acetate plus ionomycin, imiquimod, poly I:C or retinoic acid (Figure 28B). R1 macrophages expressed the receptor for leukemia inhibitory factor (LIF), but treatment of cultured BMDMs with LIF did not restore VISTA expression. In contrast, MerTK expression was not affected by *in vitro* differentiation conditions (Figure 29). Tim4 expression was lost in culture conditions, but it is known to be regained upon return to *in vivo* conditions.[17] Indeed, when I administered cultured BMDMs into the peritoneal cavity of congenic mice, the expression of Tim4 was restored after 2 weeks (Figure 29A). VISTA expression in cultured peritoneal macrophages was similarly restored when cells were returned to *in vivo* conditions (Figure 29B).

By confirming VISTA expression being restored in the peritoneum where high VISTA-expressing tissue resident macrophage is located, the results indirectly suggest that the tissue environment shapes macrophages to express VISTA which leads to consistent expression of VISTA in kidney-resident macrophages.

Functional capacity of VISTA

Next, I further researched on the roles of $VISTA^{+}$ kidney-resident macrophages. VISTA has two functional roles in phagocytosis[48] and as an inhibitory immune checkpoint.[29] First, I confirmed the phagocytic role of $VISTA^{+}$ macrophages. When fluorescence-labelled apoptotic cells were injected into mice via the tail vein, R2 macrophages and lung interstitial macrophages phagocytosed these cells. When the phagocytic capacity was compared between wild-type and *Vsir*$^{-/-}$ mice, it was approximately 10% lower in *Vsir*$^{-/-}$ cells than in wild-type cells (Figure 30A). *In vitro*, the proportion of cells phagocytosing apoptotic cells as lower in cells from *Vsir*$^{-/-}$ mice than in cells from wild-type mice (Figure 30B). Next, I confirmed that VISTA inhibited the activation and proliferation of naïve T cells and their IFN-γ secretion (Figures 31A and 31B), which remained consistent regardless of the $CD4^{+}$ or $CD8^{+}$ T cell subset. These data indicate that $VISTA^{+}$ macrophages show increased phagocytic capacity and regulate the proliferation of T cells compared with $VISTA^{-}$ macrophages.

Before IRI, the overall cell number of T cells and their subsets did not differ between wild-type and *Vsir*$^{-/-}$ mice (Figure 32). Following IRI, *Vsir*$^{-/-}$ mice showed a higher mortality rate than wild-type mice (Figure 33A). Evaluation of surviving mice revealed delayed recovery in *Vsir*$^{-/-}$ mice compared with wild-type mice (Figure 33B and Table 4). Tubules in *Vsir*$^{-/-}$ mice displayed more dilatation, casts and flattening than those in wild-type mice at 96 h following IRI (Figure 33C). These data indicated that loss of VISTA delayed the repair from IRI. At 96 h after IRI, the numbers of infiltrated $CD4^+$ and $CD8^+$ T cells were higher in *Vsir*$^{-/-}$ mice than in wild-type mice (Figure 34A), of which $CD44^-$ T cells were primarily affected (Figure 34B). Thus, the aggravation of injury in *Vsir*$^{-/-}$ mice may be attributable to the insufficient clearance of apoptotic cells and inappropriate regulation of T cell activation and proliferation.

VISTA$^+$ macrophage in human kidney

VISTA expression in human kidneys in normal conditions has not been evaluated. A total of 11 human kidneys were evaluated for VISTA expression. The mean age was 66 ± 15 years old. Nine patients (81.8%) were male. The mean values of serum creatinine and estimated glomerular filtration rate were 1.0 ± 0.2 mg/dL and 76.7 ± 19.8 mL/min/1.73 m^2, respectively. Other baseline information is described in Table 5. The characterization of human macrophages including kidney-resident macrophages is scarce,[49] and therefore specific surface markers for distinguishing subsets

have not been established. $CD14^+$ cells may include most macrophages, whereas $CD14^-$ cells represent myeloid dendritic cells.[49—51] When $CD45^+$ $CD14^+$ cells were gated after excluding dead cells and contaminated polymorphonuclear cells ($CD16^{++}$ cells), three subsets were observed based on CD33 and HLA-DR expressions (Figure 35A). Compared with peripheral blood mononuclear cells in which $CD33^+$ $HLA-DR^+$ cells were the dominant population, both $CD33^+$ $HLA-DR^+$ and $CD33^+$ $HLA-DR^-$ cells comprised most of the kidney macrophages (Figure 35B). All the $CD14^+$ cells had phagocytic capacity (Figure 35C); cell morphologies are shown in Figure 35D.

VISTA expression was observed in $CD33^+$ $HLA-DR^+$ and $CD33^+$ $HLA-DR^-$ cells, but not in $CD33^-$ $HLA-DR^-$ cells (Figure 36A). Approximately 40%—50% of $CD33^+$ $HLA-DR^+$ and $CD33^+$ $HLA-DR^-$ cells expressed VISTA in normal kidney tissue. Similar expression patterns between $CD33^+$ $HLA-DR^+$ and $CD33^+$ $HLA-DR^-$ cells were observed with regard to CD11c, CD11b, CD64, CX3CR1, CD1c and SIRPα (Table 6). A minor subset of $CD33^+$ $HLA-DR^+$ cells expressed CD68, MerTK and CD206. None of the $CD14^+$ cells expressed PD-L1 or PD-L2. Kidney-resident T cells and their subpopulations did not express VISTA (Figure 36B). The proliferation rate of human T cells cultured on a human VISTA-Fc-coated plate was reduced compared with cells cultured on a control-Fc-coated plate (Figure 37). These data indicated that many human

kidney macrophages expressed VISTA, which has similar *in vitro* functions to the mouse counterpart.[29]

Ⅳ. DISCUSSION

A confirmation of the resident immune-cell composition is required to improve our knowledge of the kidney-homeostasis, inflammation and target-immune therapy. Kidneys have a distinct immune system, and thus, subsets of resident immune cells are different from those in other organs.[52,53] The present exploratory study did not determine the mechanisms related to the high abundance of T cells within human kidneys. Decreased numbers of other immune-cell subsets might lead to an increase in T cells. In addition to this simple hypothesis, I focused on the relatively high proportion of T_{RM}. Non-lymphoid tissues such as kidneys harbor certain populations of memory T cells that are not present in the circulation (referred to as T_{RM}), which are different from circulating T cells.[54] The cytokine milieu after inflammatory insults, such as infections or ischemic damage, drives the development of T_{RM}, and thus, mouse kidneys in the present study had few T_{RM} in the absence of kidney insults. In contrast to mouse conditions, the study subjects might have experienced subclinical injury although most of their kidney functions were within the normal range. Furthermore, continuous contact with uremic toxins, spontaneously-dead parenchymal cells or debris from tubules and glomeruli over the years might affect the development of the T_{RM} subset.[55] The different splenic immune cell profiles between wild and laboratory mice supports the hypothesis that the environmental milieu alters the renal immune cell composition.[56] Intriguingly,

$CD49a^+$ cells were the predominant $CD4^+$ and $CD8^+$ T_{RM} subsets, but CD103 was not the primary marker of kidney T_{RM}. This feature is different from the phenotype and distribution of T_{RM} subpopulations in other peripheral organs.[37] The characteristics of renal epithelial cells and their adhesion molecules may determine the markers of T_{RM}, which will be addressed in another project.

Kidneys contain specialized resident-macrophages that monitor and scavenge the endothelial transport of immune complexes, and subsequently trigger type III hypersensitivity responses.[39] These phenomena may be crucial in diseases attributable to the insufficient clearance of immune complexes.[57] The proangiogenic activity of kidney-resident macrophages during renal artery stenosis was also reported.[58] This frontline and potential homeostatic activity of resident-macrophages may be related to their high proportion in mouse kidneys. However, the residency and proportion of resident-macrophages have not been fully evaluated in human kidneys. Recent single-cell RNA sequencing data suggested that markers such as CD74 and CD81 might characterize human kidney-resident macrophages.[59] However, these markers are also expressed on other myeloid subsets of that dataset or on non-myeloid cells.[60] Accordingly, the present study used conventional myeloid markers such as CD14, CD64, HLA-DR, and CD68 to identify macrophages and monocytes. In human kidneys, approximately 10% of total resident immune cells were identified as macrophages, where they had an expression of CD64 and HLA-DR whilst being absent of CD16.

The proportion of cDCs was 1.1%. Therefore, macrophages exhibited the highest proportion in myeloid cells of the human kidney. In mouse kidneys, kidney resident macrophages were the highest proportion of resident immune cells. These results suggest that tissue resident macrophages play a role as antigen presentation cells affecting the regulation of T_{RM} through constant direct cell to cell contact. Moreover, the tissue-resident macrophages seem to regulate kidney homeostasis and inflammation.

Therefore, I was performed in order to verify the effect of tissue-resident macrophage on homeostasis and renal injury. The origin and development of tissue-resident macrophages have been well characterized,[61,62] but their roles during homeostasis or inflammation are less defined, particularly in the kidney. The present study provides insight into kidney macrophages, which include resident (R1) and infiltrating monocyte-derived (R2) subsets. These subsets may contribute a balanced cooperation during renal inflammation, whereas insufficient repair from ischemic injury occurs if the R1 subset is depleted. Repair is mediated by R1 macrophages highly expressing VISTA on their surface. VISTA expression is tissue-specific and thus kidney-dependent. A substantial proportion of human macrophages also express VISTA, which may promote repair in the human kidney environment.

Gene transcription in macrophages is regulated in a tissue- and lineage-specific manner, as observed with *Sall1* (brain), *Spi-c* (spleen), *Clec4f* (liver), *Car4* (lung), *Tfgb2* (peritoneum) and *Runx3*

(intestine).[20] However, detailed information is not available for kidney macrophages. The kidney environment also shapes the gene transcription profiles of two macrophage subsets, which may provide different functions to each subset. This idea is supported by the present sequencing data, wherein R1 and R2 macrophages were associated with chemotaxis of leukocytes and the response to inflammation, respectively. Each macrophage subset has its own functions.[23,49] R1 macrophages monitor the transport of immune complexes into the interstitial space and phagocytose them.[23] R2 macrophages respond to bacterial inroad and subsequently increase the inflammatory signals for the defense against infection.[49] Both macrophage subsets may participate in maintaining kidney homeostasis after ischemic injury while R2 macrophages were likely to infiltrate during renal inflammation. Their proportion was lower than that of R1 macrophages in normal mouse kidney. Also, infiltrating macrophages produce large amounts of pro-inflammatory cytokines, which are involved in tissue injury.[63] Therefore, I researched about R1 macrophages with characteristics of tissue residence which play a dominant role in maintaining tissue homeostasis and repairing tissue after ischemic injury.

Each tissue harbors various subsets of macrophages, similar to the kidney. For example, normal lung tissue harbors three macrophages subsets; alveolar, interstitial and vascular macrophages.[64] Several subsets have also been evaluated in other organs such as intestine and skin[13,65] and their functional properties

can vary according to the disease status.[14] My results indicate that in the present IRI model, R1 macrophages participated in the repair process, although several caveats of macrophage-depleting experiments should be considered such as functional differences in the repopulating subsets, co-depletion of dendritic cells, and potential aggravation of inflammatory conditions by CL. R1 and R2 subsets may be regarded as uncommitted macrophages, and if inflammatory insults are introduced, they may polarize their phenotypes into the M1 or M2 subset, based on the macrophage subtype nomenclature system.[66] However, discrimination between M1 and M2 is primarily recognized in the *in vitro* environment, but functional plasticity in the *in vivo* environment may be different. IRI damage was abrogated following depletion of total macrophages, which supports a previous report.[45] This suggests that R1 macrophages may also participate in initiating inflammation, irrespective of phenotypic plasticity. Considering their role in repair after IRI, R1 macrophages may function with an M1 or M2 phenotype, depending on the tissue environmental characteristics, which supports the concept of phenotypic or functional plasticity of kidney macrophages.[66,67]

VISTA has primarily been explored in cancer immunology[29] and under non-infectious conditions such as autoimmunity.[46] Recent human data on VISTA^{+} macrophages provided insight into the polarized immune response by their tissue residency, but the understanding is limited because these studies focused on tumor

microenvironment-specific functions.[47,68] Previous studies have shown that VISTA is also induced after inflammatory insults.[47] However, the present data revealed that kidney macrophages substantially expressed VISTA even under normal conditions in the absence of insult. Constitutive expression of negative immune checkpoint molecules has also been shown in follicular T helper (Tfh) cells, which express programmed cell death protein 1 (PD-1) in germinal centers. PD-1 expression determined the localization and function of Tfh cells during the germinal center response.[69] In addition, cytotoxic T-lymphocyte associated protein 4 (CTLA-4) in regulatory T cells maintained intestinal homeostasis by preventing hyperactivation of T cells.[70] VISTA displays two functional roles as a phagocytosis receptor and as an inhibitory immune checkpoint molecule, which may boost the repair capacity of R1 macrophages and maybe also in some R2 macrophages following ischemic injury. The differential expression of VISTA between the two macrophage subsets might be related to their functional characteristics. This finding may be translated into several species, as VISTA is evolutionally conserved.[29] A substantial proportion of human kidney macrophages (especially $CD14^+CD33^+$ cells) also expressed VISTA even under normal conditions. Thus, VISTA can be used as an important biomarker for discriminating different kidney macrophage subsets, because CD68, a traditional macrophage marker, is a *bona-fide* intracellular antigen and is expressed only in a minor subset of kidney macrophages.[49] Future studies exploring the use VISTA for

determining the role of human macrophages and evaluating the specific lineage of macrophages in various pathologic conditions are needed.

In conclusion, I investigated composition of immune cells in kidney and a role of kidney-resident macrophages in the repair from ischemic injury. As a molecule related with repair, VISTA is identified. This is constitutively expressed in kidney macrophages as a tissue-specific manner and accelerates the repair process following ischemic injury. In addition to unraveling the function of kidney-resident macrophages, the present results will provide a basis of future development of resolution-targeting therapy from ischemic renal injury.

Table 1. Baseline characteristics of human subjects for analysis of immune-cell composition in kidney.

Variables	Total (n = 15)
Age (years)	69.1 ± 10.4
Male sex (%)	66.7
Diabetes mellitus (%)	13.3
Hypertension (%)	66.7
Cancer (%)	
Clear cell renal cell carcinoma	63.6
Papillary urothelial carcinoma	36.4
Blood urea nitrogen (mg/dL)	16.6 ± 4.8
Serum creatinine (mg/dL)	1.0 ± 0.3
Estimated glomerular filtration rate (mL/min/1.73 m^2)	73.6 ± 15.2
Proteinuria (%)	20.0
Hematuria (%)	20.0

Proteinuria and hematuria were defined as ≥ 1+ on a dipstick test.

Table 2. Histological findings of human subjects for analysis of immune-cell composition in kidney.

Pathologic findings	Total (n = 15)
Diabetic nephropathy (%)	13.3
Hypertensive nephropathy (%)	6.7
Tubular atrophy	
< 25%	93.3
25%—50%	6.7
> 50%	0
Interstitial fibrosis	
< 25%	6.7
25%—50%	13.3
> 50%	0

Table 3. Surface or intracellular markers of kidney R1, R2, and neutrophils.

Markers	R1	R2	Neutrophils
CD11b	+	++	+
F4/80	++	+	−
CD11c	++	+	−
CX3CR1	+	+	±
CD68	+	+	−
CD64	+	−	−
Ly6C	−	±	+
Ly6G	−	−	+
M−CSF receptor	+	+	−
GM−CSF receptor	+	+	−
ST2	−	−	−
B220	−	−	−
XCR−1	−	−	−
CCR2	±	±	−
CCR5	−	−	−
CCR7	−	−	−
IL−10 receptor	±	±	−
MerTK	+	−	−
TIM4	−	−	−
MHC class II	++	±	−
Zbtb46	−	−	−

Table 4. Mean values and standard deviations of blood urea nitrogen and creatinine after ischemia–reperfusion injury.

Parameter	Timeframe (days)	Figure 17A			Figure 33B		
		PL	CL	*P*	WT	*Vsir*$^{-/-}$	*P*
BUN	1	112.6 ± 52.5	124.5 ± 37.7	0.673	138.1 ± 25.3	134.8 ± 19.4	0.841
	2	171.0 ± 85.3	170.7 ± 52.4	0.993	170.7 ± 46.6	183.0 ± 44.3	0.664
	3	42.9 ± 19.4	85.0 ± 37.7	0.009	45.0 ± 8.4	80.4 ± 9.9	0.004
	4	42.5 ± 11.3	67.4 ± 20.4	0.003	36.8 ± 7.5	56.6 ± 9.2	0.004
Creatinine	1	0.9 ± 0.3	0.9 ± 0.3	0.709	1.3 ± 0.2	1.2 ± 0.3	0.904
	2	1.7 ± 0.6	1.5 ± 0.3	0.413	1.8 ± 0.3	2.2 ± 0.3	0.088
	3	0.6 ± 0.3	1.0 ± 0.5	0.043	0.4 ± 0.1	0.8 ± 0.1	0.006
	4	0.4 ± 0.1	0.6 ± 0.2	0.024	0.4 ± 0.1	0.6 ± 0.1	0.016

PL, PBS liposome; CL, clodronate liposome; WT, wild type; BUN, blood urea nitrogen.

Table 5. Baseline characteristics of human subjects for human macrophage analysis.

Variables	Total (n = 11)
Age (years)	66.4 ± 15.1
Male sex (%)	81.8
Diabetes mellitus (%)	9.1
Hypertension (%)	54.5
Blood urea nitrogen (mg/dL)	16.5 ± 4.7
Serum creatinine (mg/dL)	1.0 ± 0.2
Estimated glomerular filtration rate (mL/min/1.73 m^2)*	76.7 ± 19.8
Proteinuria (%)	18.2
Hematuria (%)	54.5

Proteinuria and hematuria were defined as ≥ 1+ on a dipstick test.
*Calculated using the Chronic Kidney Disease Epidemiology Collaboration equation.

Table 6. Representative surface or intracellular markers of human kidney myeloid subsets

Markers	Live $CD45^+$ $CD14^+$		
	$CD33^+$ HLA−DR^+	$CD33^+$ HLA−DR^-	$CD33^-$ HLA−DR^-
VISTA	++	++	−
CD16	±	±	±
CD11c	+	+	±
CD11b	++	++	−
CD68	±	−	−
CD64	++	++	−
CX3CR1	+	+	−
CCR2	+	+	−
MerTK	±	−	−
CD1c	+	+	±
SIRP α	++	++	+
CD123	+	−	−
CD206	±	−	−
PD−L1	−	−	−
PD−L2	−	−	−
CD81	+	+	±

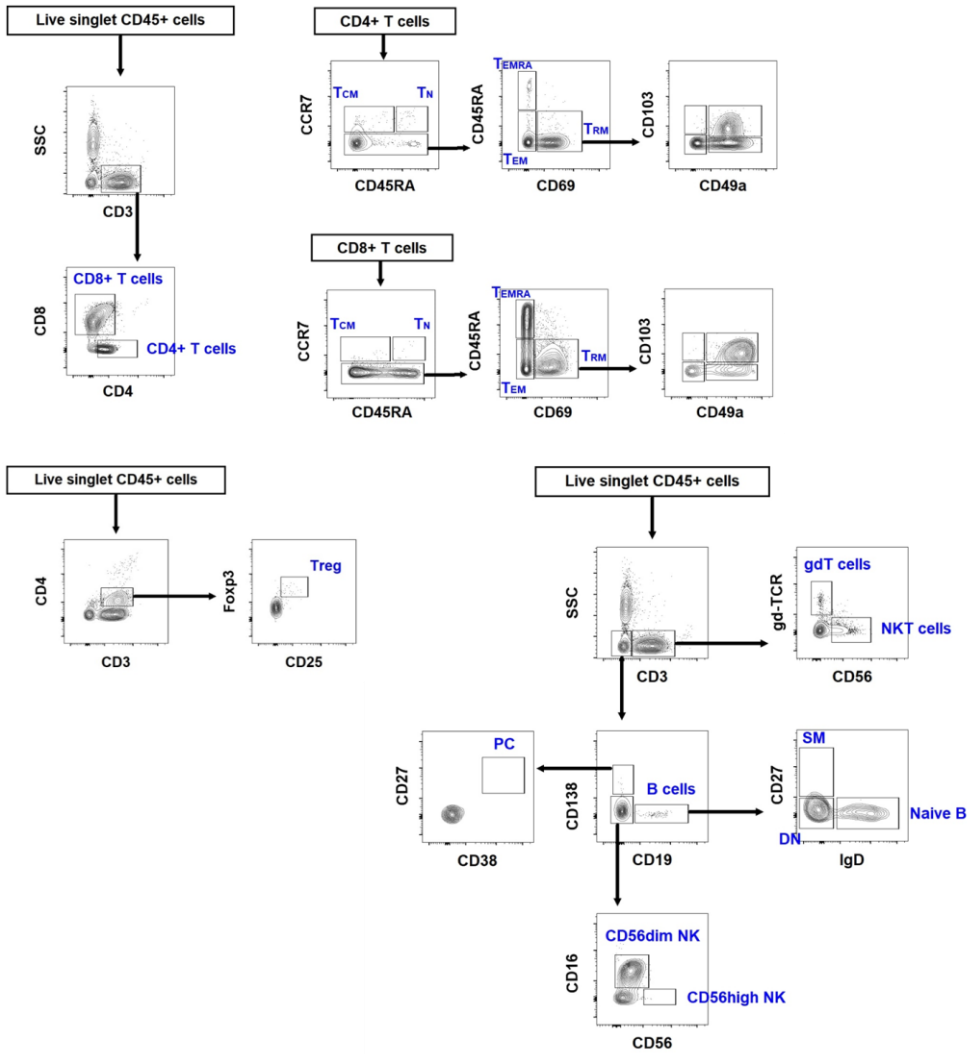

Figure 1. Gating strategy for human T cell, B cell, and NK cell subsets in kidney. Representative flow cytometry plots showing gating strategy. T_N, naïve T; T_{CM}, central memory T; T_{EM}, effector memory T; T_{EMRA}, $CD45RA^+$ effector memory T; T_{RM}, resident memory T; Treg, regulatory T; gdT, gamma/delta T; PC, plasma cell; SM, class-switched memory B; DN, IgD^- $CD27^-$ B.

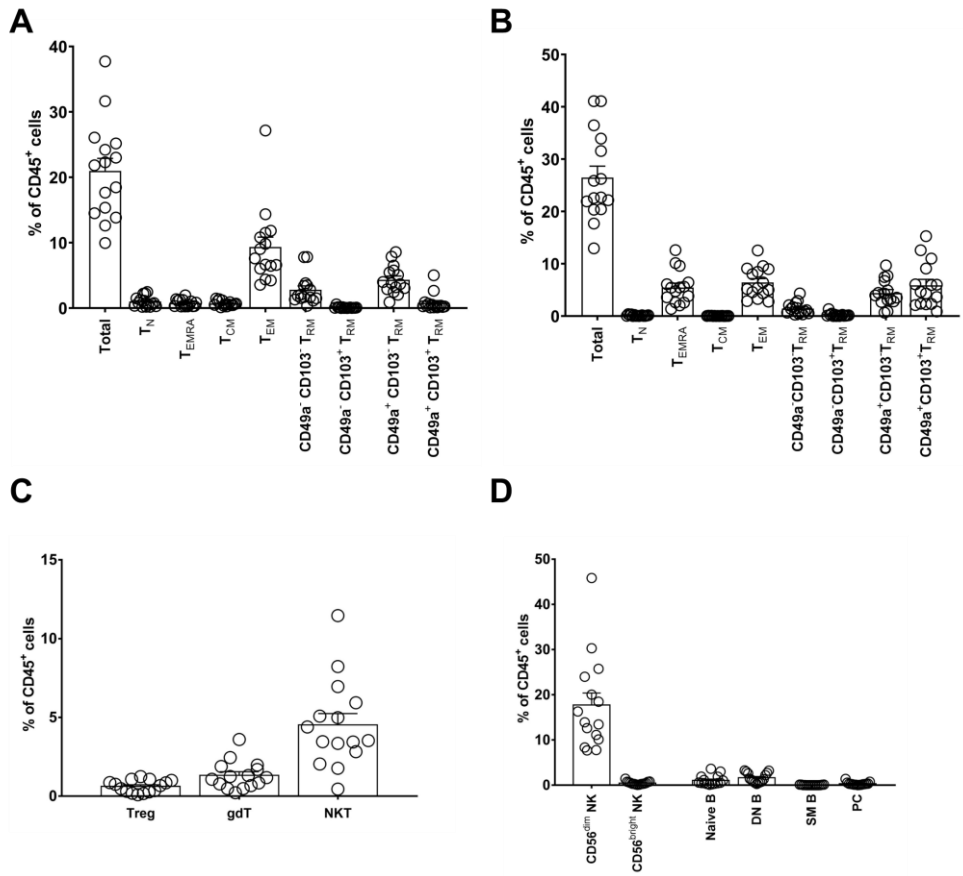

Figure 2. Lymphocytes and natural killer (NK) cells in human kidneys. (A) Proportion of the $CD4^+$ T cell subset. (B) Proportion of the $CD8^+$ T cell subset. (C) Proportions of Treg, gdT, and $CD56^+$ T cell subsets. (D) Proportions of B cell and NK cell subsets. T_N, naïve T; T_{CM}, central memory T; T_{EM}, effector memory T; T_{EMRA}, $CD45RA^+$ effector memory T; T_{RM}, resident memory T; Treg, regulatory T; gdT, gamma/delta T; PC, plasma cell; SM, class-switched memory B; DN, IgD^- $CD27^-$ B. n = 15. Data were combined from fifteen independent experiments. Bar graphs show the mean ± SEM.

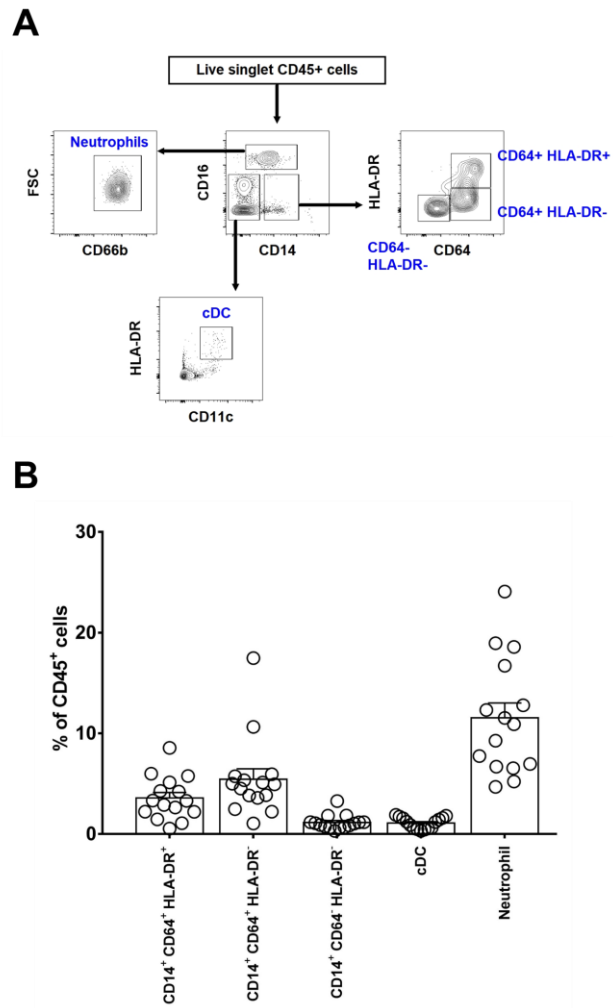

Figure 3. Myeloid cells in human kidneys. (A) Gating strategy for kidney macrophage, classical dendritic cell (cDC), and neutrophil subsets. (B) Proportion of myeloid cell subsets in human kidneys. *n* = 15. Data were combined from fifteen independent experiments. Bar graphs show the mean ± SEM.

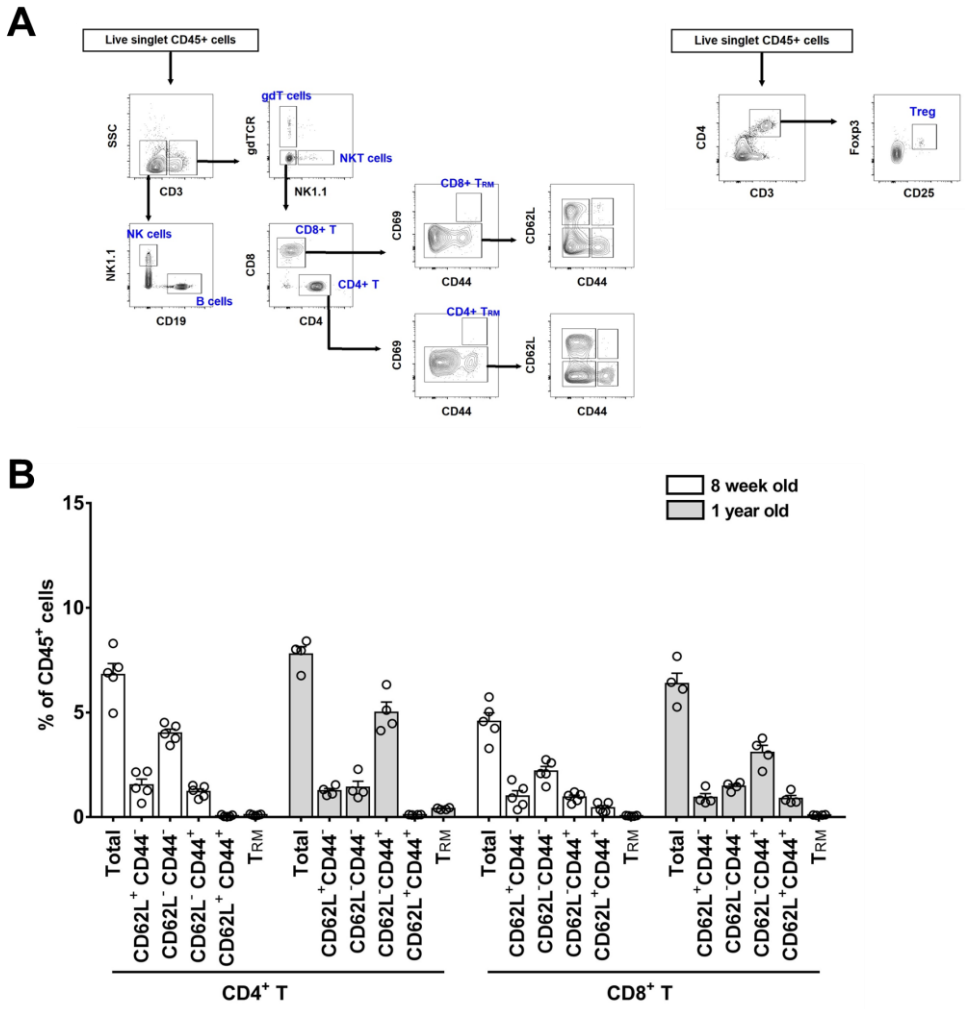

Figure 4. Lymphocytes and natural killer (NK) cells in mouse kidneys. (A) Gating strategy for kidney T cell, B cell, and NK cell subsets. (B) Proportion of the T cell subset. Harvested kidneys from 8-week- and 1-year-old B6 mice were evaluated after perfusion with 10 mL of cold PBS via the left chamber of the heart. Bar graphs show the mean ± SEM. T_{RM}, resident memory T; Treg, regulatory T. n = 4~5 per group. Data were combined from three independent experiments.

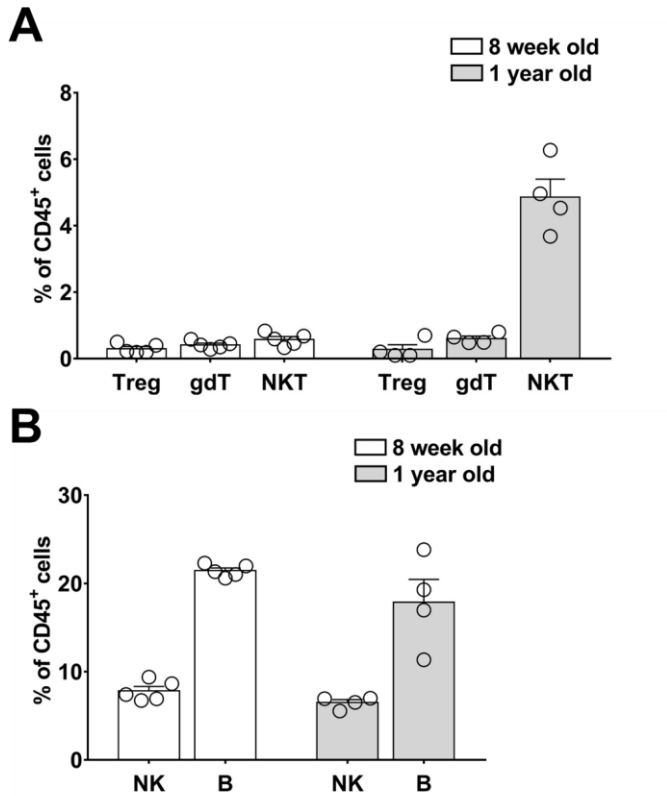

Figure 5. Proportion of other immune cells in mouse kidney. (A) Proportions of Treg, gdT, and NKT cell subsets. (B) Proportions of B cell and NK cell subsets. Harvested kidneys from 8-week- and 1-year-old B6 mice were evaluated after perfusion with 10 mL of cold PBS via the left chamber of the heart. Bar graphs show the mean ± SEM. n = 4~5 per group. Data were combined from three independent experiments. γδT, gamma/delta T; Treg, regulatory T.

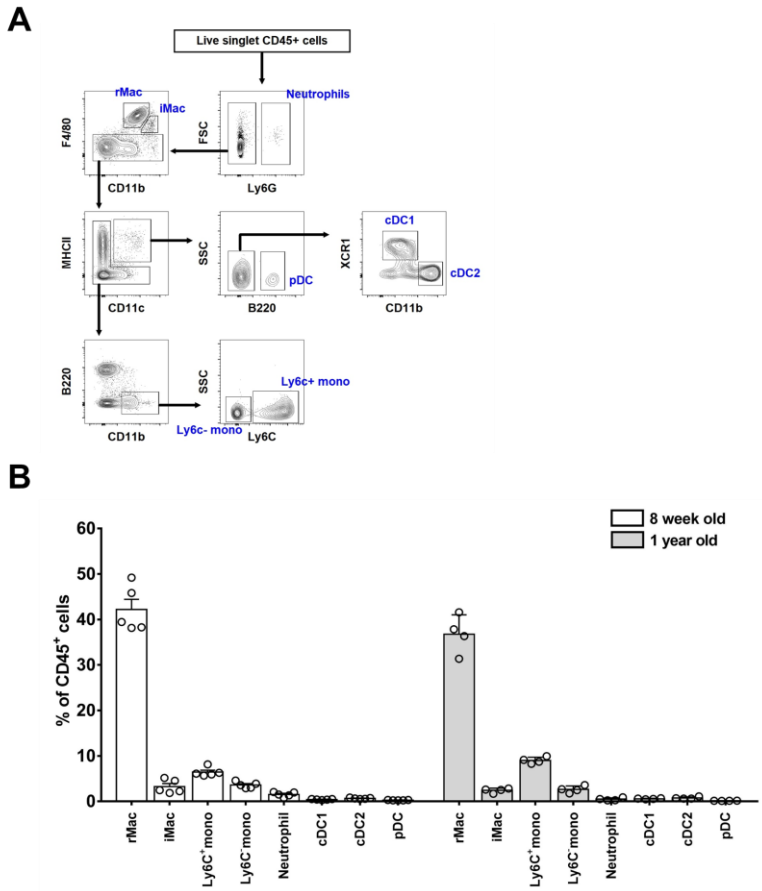

Figure 6. Myeloid cells in mouse kidneys. (A) Gating strategy for kidney monocyte (mono), resident and infiltrating macrophages (rMac and iMac, respectively), classical and plasmacytoid dendritic cells (cDCs and pDCs, respectively), and neutrophil subsets. (B) Proportion of myeloid cell subsets in mouse kidneys. Harvested kidneys from 8-week- and 1-year-old B6 mice were evaluated after perfusion with 10 mL of cold PBS via the left chamber of the heart. Bar graphs show the mean ± SEM. n = 4~5 per group. Data were combined from three independent experiments.

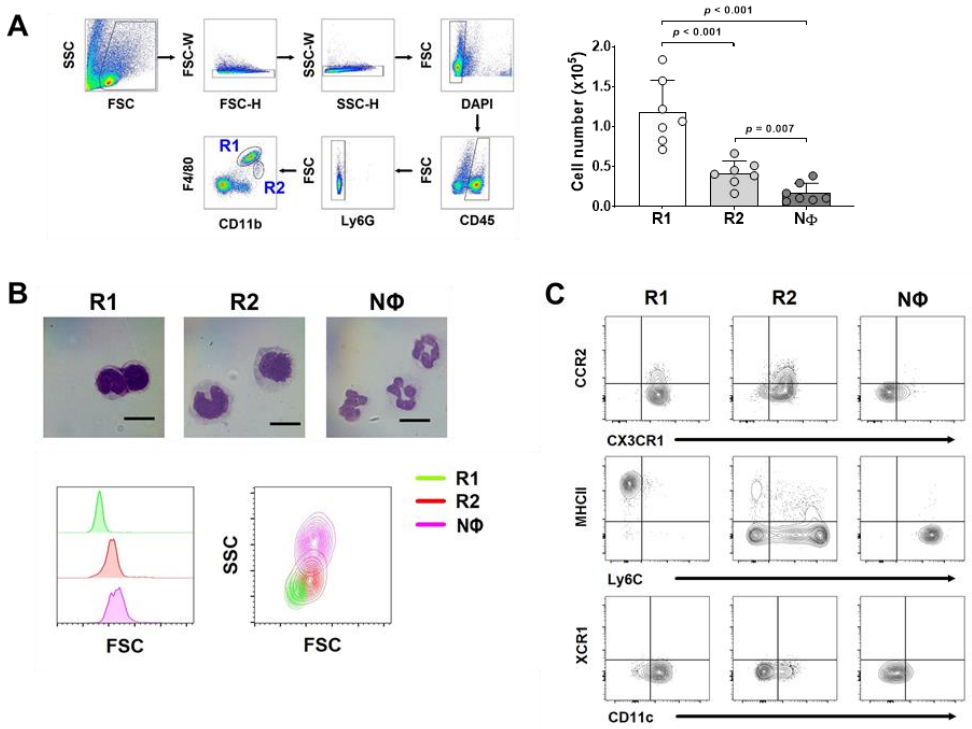

Figure 7. Two subtypes of kidney macrophages. (A) The gating strategy for kidney macrophages and cell numbers. Data were combined from three independent experiments. (B) Giemsa staining of kidney macrophages and Nϕ. Scale bar = 10 μm. Relative cell size was compared between subsets using forward scatter intensity (FSC). (C) Representative surface markers of kidney R1, R2 and Nϕ subsets. Nϕ, neutrophils. Representative results from three independent experiments (n = 2/experiment). Bar graphs show the mean ± SEM and p-values were obtained using a two-tailed Student's t test.

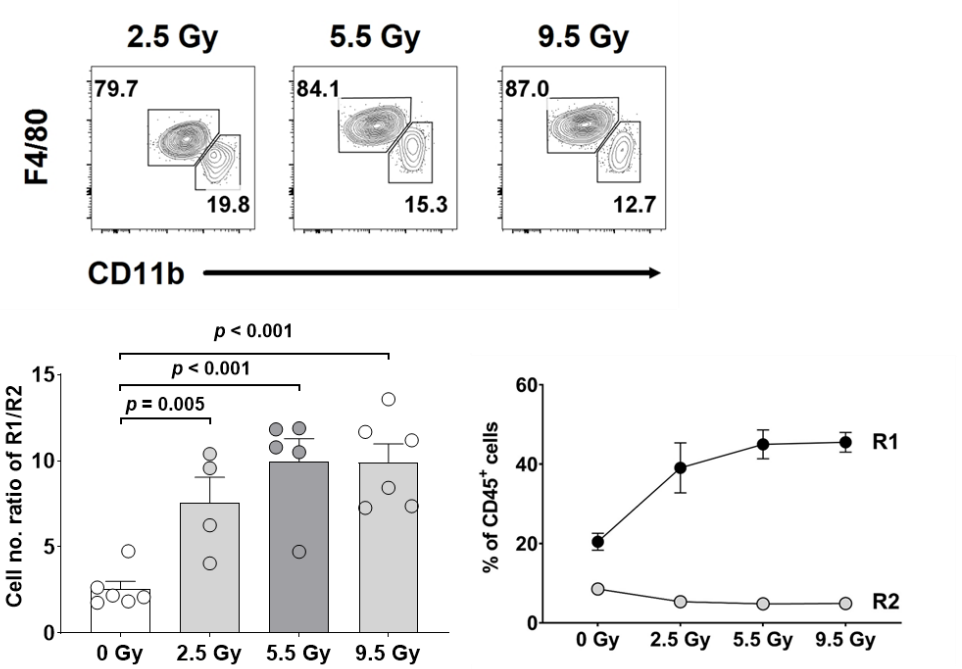

Figure 8. Radiation resistance in R1 and R2 macrophages. Representative flow cytometry plot, cell number ratio, and proportions of R1 and R2 macrophages are shown. Data were combined from three independent experiments (n = 2/group/experiment). Bar and line graphs show the mean ± SEM. p-values were obtained using a two-tailed Student's t test.

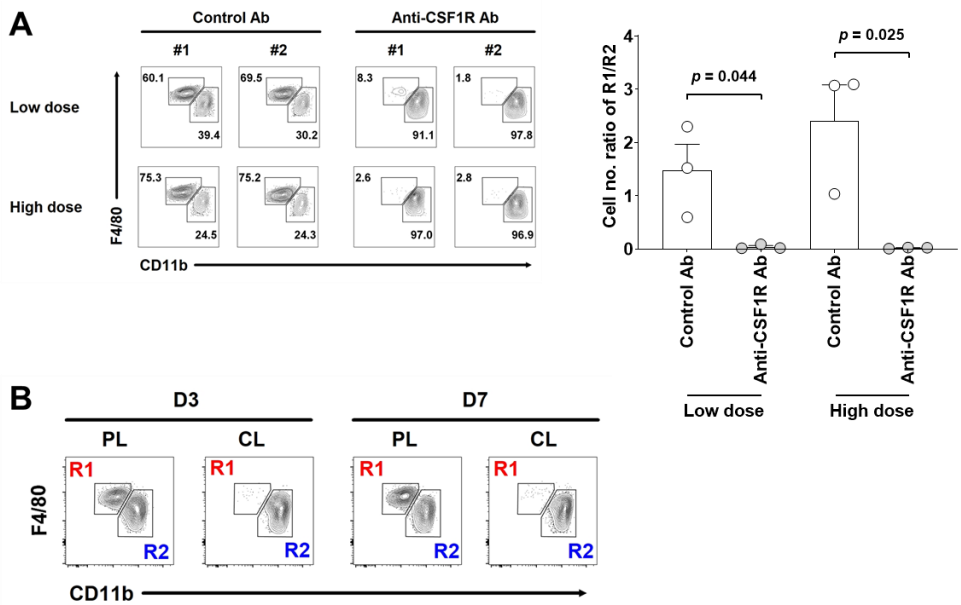

Figure 9. The depletion kinetics of R1 macrophages by anti-CSF-1 receptor Abs or clodronate liposomes. (A) Depletion of R1 and R2 macrophages by anti-CSF1R Abs. Representative flow cytometry plot and cell number ratio of R1 and R2 macrophages are shown. Data were combined from three independent experiments (n = 1/group/experiment). Bar graphs show the mean ± SEM and p-values were obtained using a two-tailed Student's t test. (B) Depletion of R1 and R2 macrophages by clodronate liposomes (CL) compared with PBS liposomes (PL). Cells were gated from the $DAPI^-$ $CD45^+$ $Ly6G^-$ $CD11b^+$ $F4/80^+$ subset. Representative results from three independent experiments (n = 2/group/experiment).

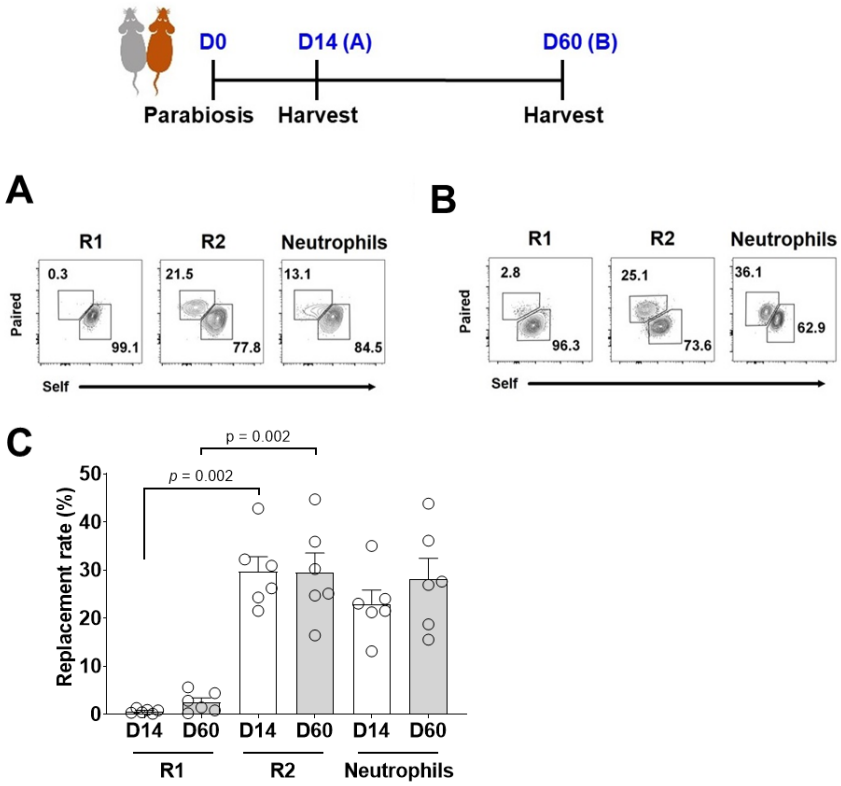

Figure 10. Replacement rates of R1, R2 and Nϕ. Replacement of kidney-resident macrophages by infiltrating mono/macrophages at day 14 (A) and day 60 (B) after parabiosis. Representative flow cytometry plot from one of three independent experiments. (C) Bar graph for the replacement rates. Cells were gated from the $DAPI^{-}$ $CD45^{+}$ $Ly6G^{-}$ $CD11b^{+}$ $F4/80^{+}$ subset. Bar graphs show the mean ± SEM. Data were combined from three independent experiments (n = 2/group/experiment). p-values were obtained using a two-tailed Student's t test.

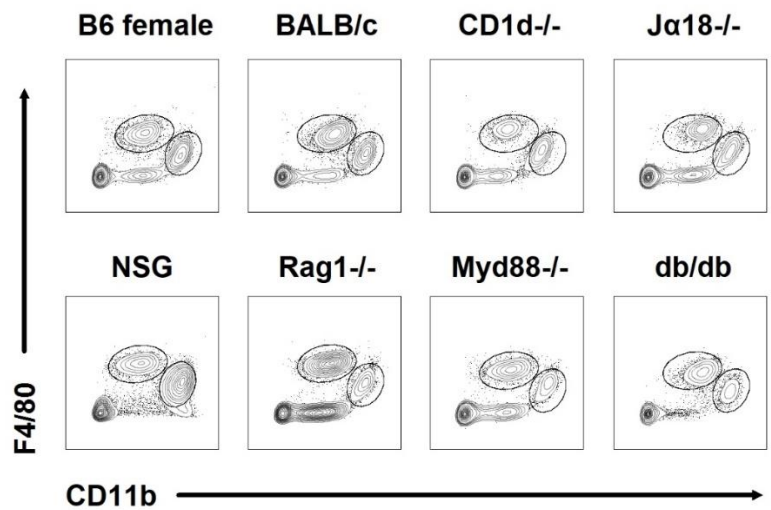

Figure 11. Development of kidney-resident macrophages. Representative flow cytometry plots from one of three independent experiments (n = 1/group/experiment). Cells were gated from the DAPI$^-$ CD45$^+$ Ly6G$^-$. CD11b^{int} F4/80^{high}(R1) and CD11b^{high} F4/80^{int} (R2) macrophages. NSG, NOD/SCID-gamma null mouse.

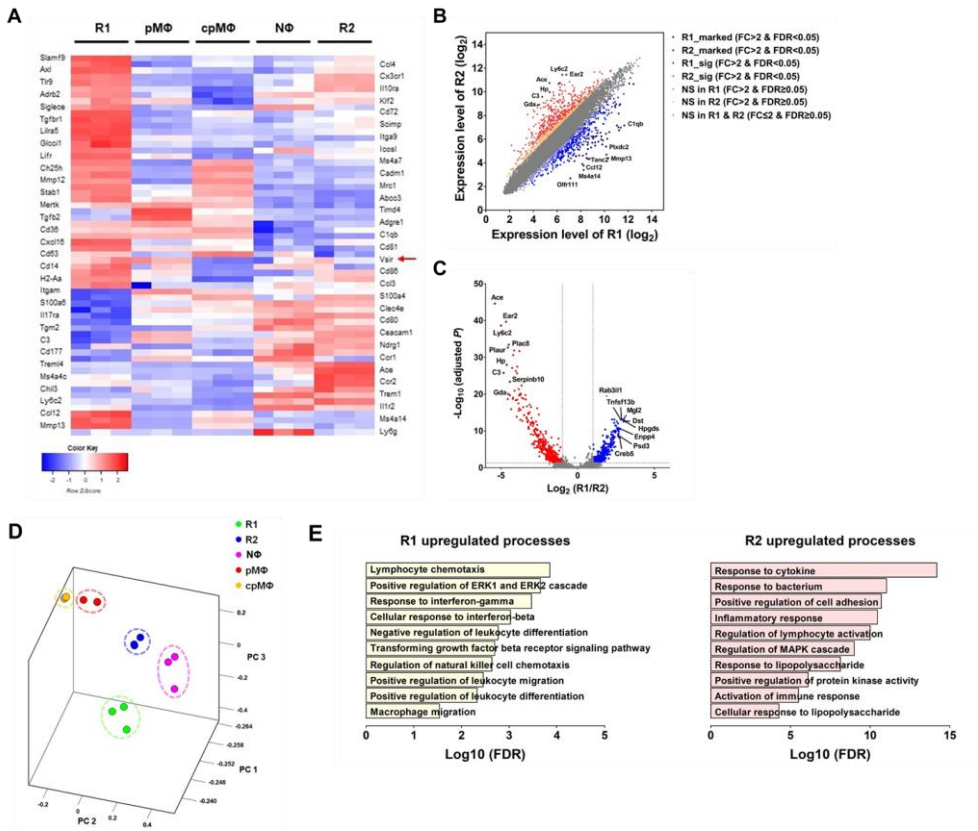

Figure 12. Transcriptomic profiling of R1 and R2 macrophages. (A) Gene expression profile of kidney R1 and R2 macrophages, Nϕ, peritoneal macrophages (pMϕ) and *in vitro* cultured pMϕ (cpMϕ). Each column represents a sample and each row represents a transcript. Scatter (B) and volcano (C) plots of microarray to differentiate between two subsets of kidney macrophages (D) Principal component analysis of five subsets. (E) Gene set enrichment assay for R1 and R2 macrophages. Data (B, C, E) were combined from three samples.

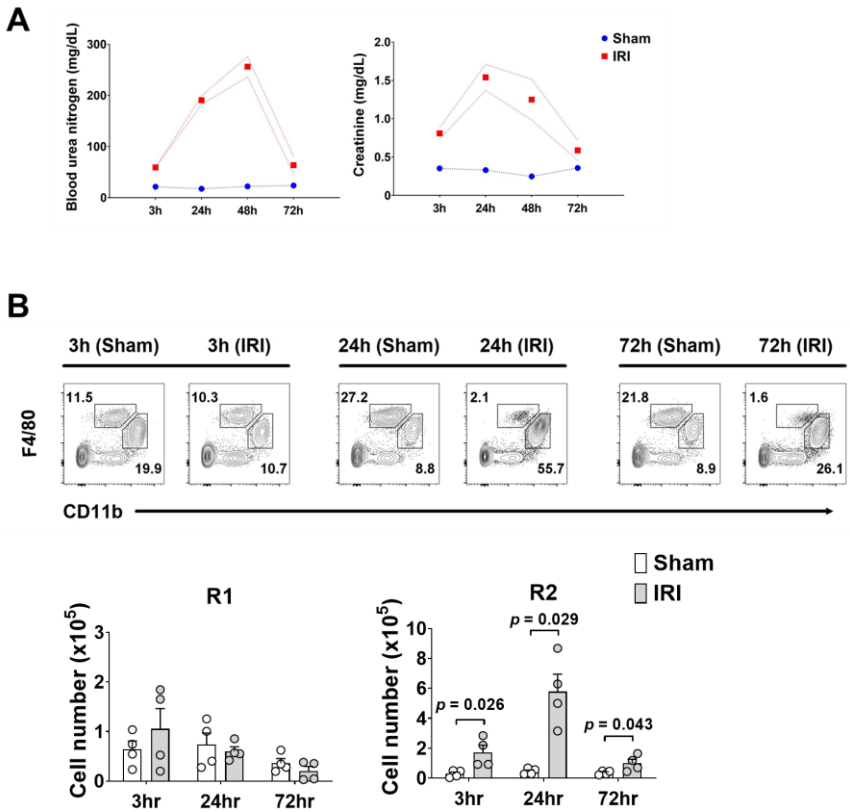

Figure 13. IRI at bilateral kidney. (A) Kinetics of kidney injury parameters after ischemia–reperfusion injury (IRI). Data were combined from two independent experiment (n = 2/group/experiment). (B) Proportion and cell number (per kidney) of R1 and R2 macrophages after IRI. Cells were gated from the DAPI$^-$ CD45$^+$ Ly6G$^-$ subset. Bar graphs show the mean ± SEM. Data were combined from three independent experiments (n = 1~2/group/experiment). p–values were obtained using a two–tailed Student's t test.

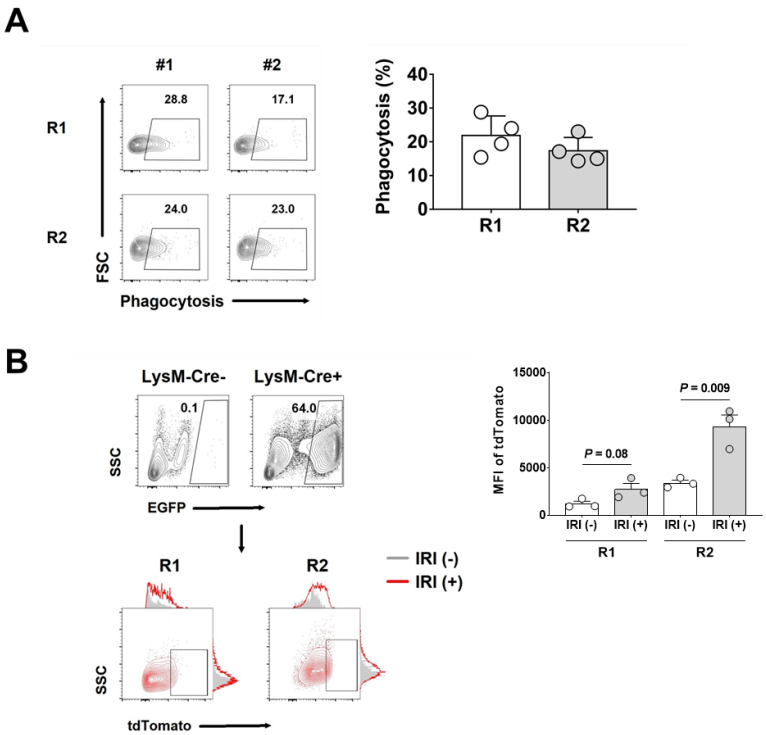

Figure 14. Phagocytic activity of R1 and R2 macrophages. (A) Phagocytosis of kidney macrophages in single cell suspension assay at 24 h after IRI. n = 4 per group. (B) Phagocytic activity of kidney macrophages before (gray) and at 48 h after (red) IRI in *LysM-Cre-Rosa26-mTmG* mice. *Rosa26-mTmG* mice (upper panel, *LysM-Cre*$^{-}$) were used to define EGFP autofluorescence (0% of cells above the EGFP threshold). Relative phagocytic activity was quantified using the mean fluorescence intensity (MFI) of tdTomato within each macrophage group. n = 3 per group. Bar graphs show the mean ± SEM. Data were combined from two independent experiments (n = 1~2/group/experiment). p-values were obtained using a two-tailed Student's t test.

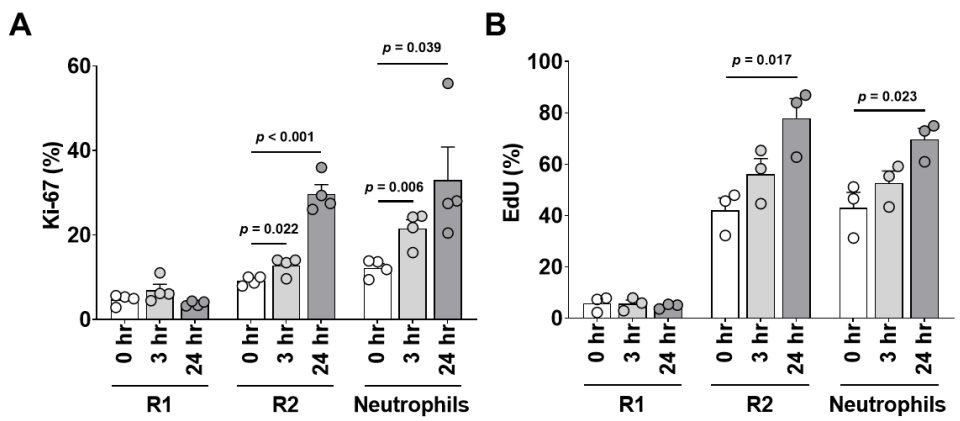

Figure 15. Proliferation capacity of kidney macrophages. Proliferation rate was determined by Ki-67 expression (A) and Click-iT EdU assay (B). n = 3~4 per group. Bar graphs show the mean ± SEM. Data were combined from two independent experiments (n = 1~2/group/experiment). p-values were obtained using a two-tailed Student's t test.

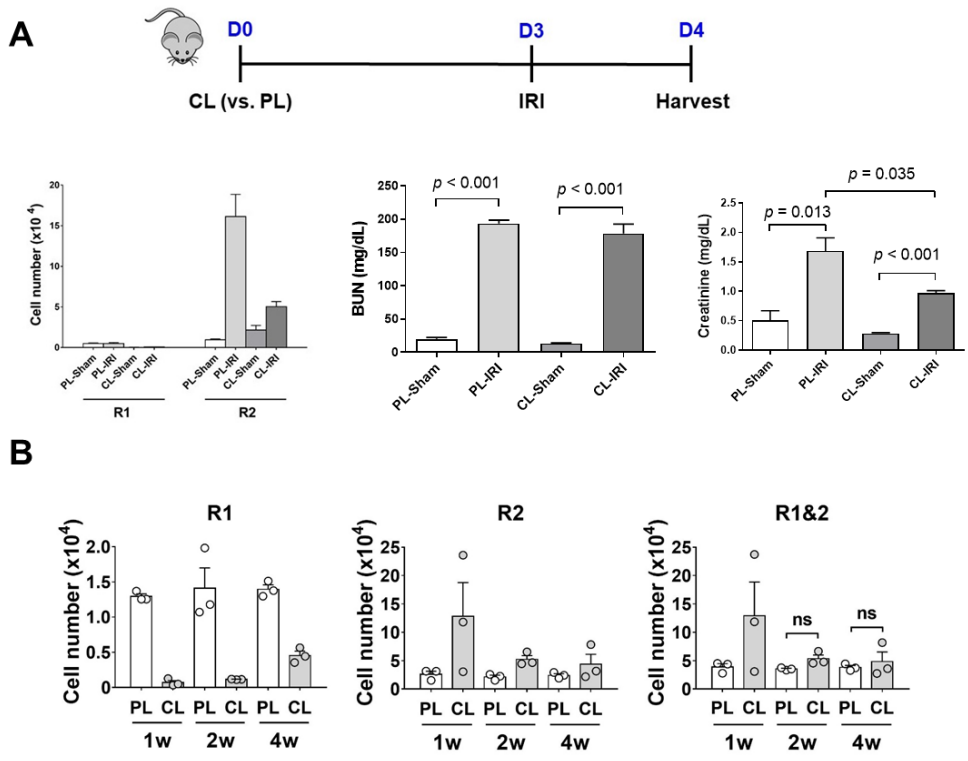

Figure 16. Ischemic injury after depletion of kidney macrophages.
(A) Ischemic injury induced at early time point after depletion of kidney macrophages. Cell number (per kidney) and Kidney injury parameters such as blood urea nitrogen (BUN) and creatinine after IRI in CL-treated and PL-treated mice. n = 3 per group. (B) Kinetics analysis of kidney macrophages cell number (per kidney) after injection clodronate liposome. n = 3 per group. Bar graphs show the mean ± SEM. All data (A, B) were combined from three independent experiments (n = 1/group/experiment). p-values were obtained using a two-tailed Student's t test. CL, clodronate liposome; PL, PBS liposome; IRI, ischemia-reperfusion injury.

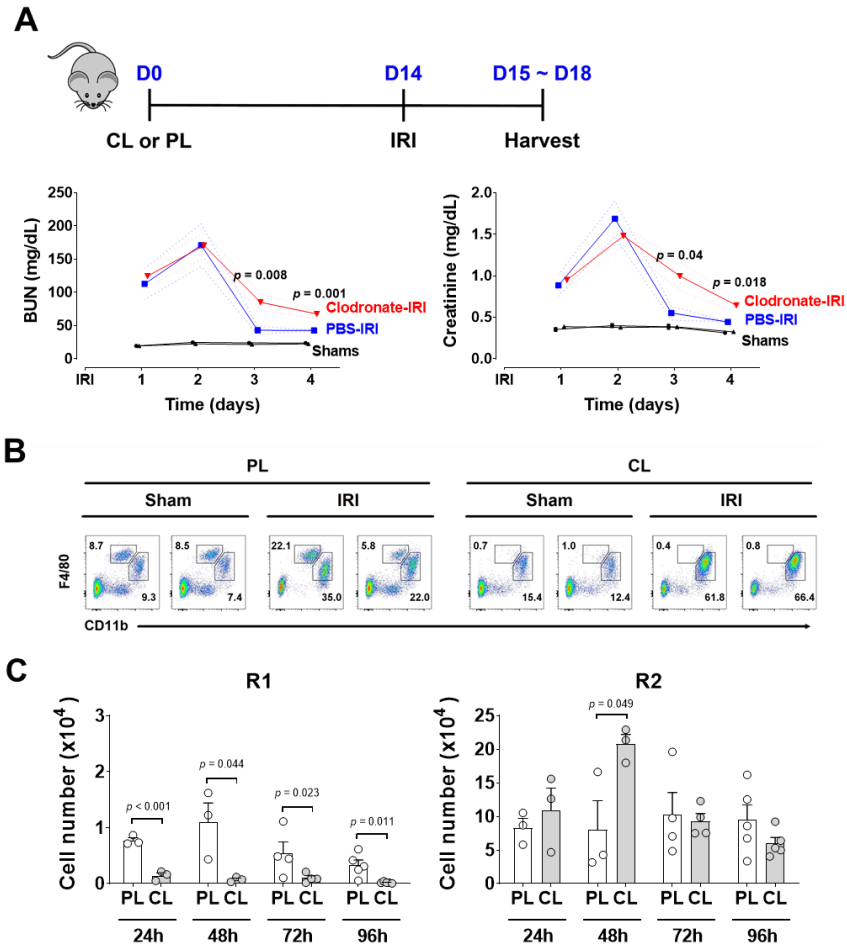

Figure 17. Resolution of ischemic injury by kidney-resident macrophages. (A) Kinetics of kidney injury parameters such as blood urea nitrogen (BUN) and creatinine after IRI in CL-treated (i.e., R1-depleted) and PL-treated mice. n = 8~10 per group. Data were combined from three independent experiments (n = 3/group/experiment). (B) Representative flow cytometry plot at 48 h after injury. Cells were gated from the $DAPI^-$ $CD45^+$ $Ly6G^-$ subset. Representative results from three independent experiments. (C) Macrophage cell number (per kidney) after IRI. n = 3~5 per group. Bar graphs show the mean ± SEM. Data were combined from two independent experiments (n = 2/group/experiment). p-values were obtained using a two-tailed Student's t test. CL, clodronate liposome; PL, PBS liposome; IRI, ischemia-reperfusion injury.

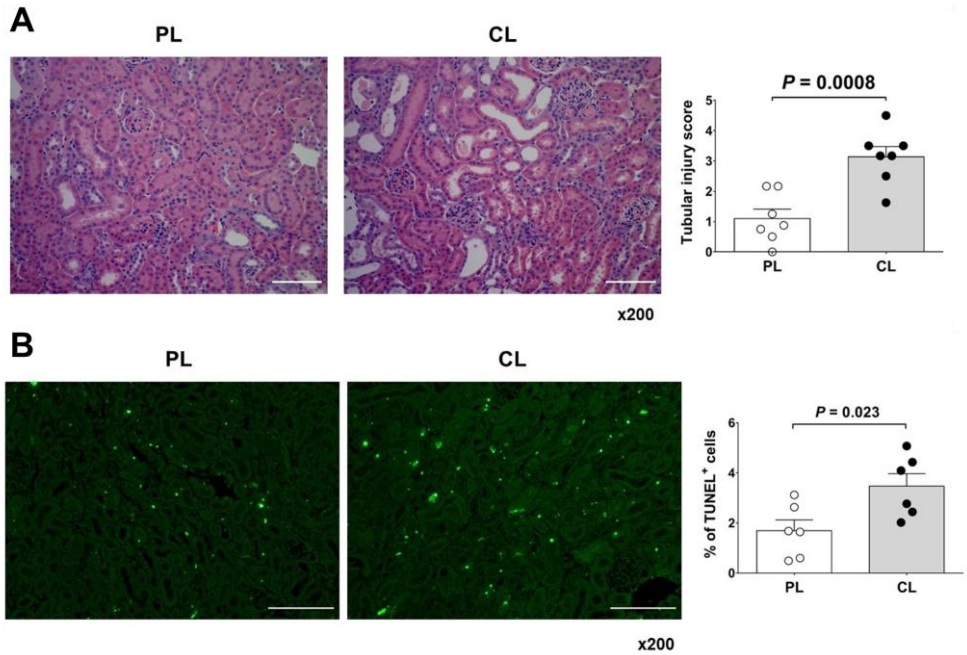

Figure 18. R1-depleted mice showed tubular damage and harbored apoptotic cells. Resolution of ischemic injury by kidney-resident macrophages. (A) Representative H&E images at 96 h after IRI. Tubular injury score was calculated based on 10 randomly selected images. Scale bar = 100 μm. (B) Representative TUNEL images at 96 h after IRI. TUNEL$^+$ cells were calculated based on 10 randomly selected images. Scale bar = 100 μm. Bar graphs show the mean ± SEM. All data (A, B) were combined from three independent experiments (n = 2~3/group/experiment). p-values were obtained using a two-tailed Student's t test.

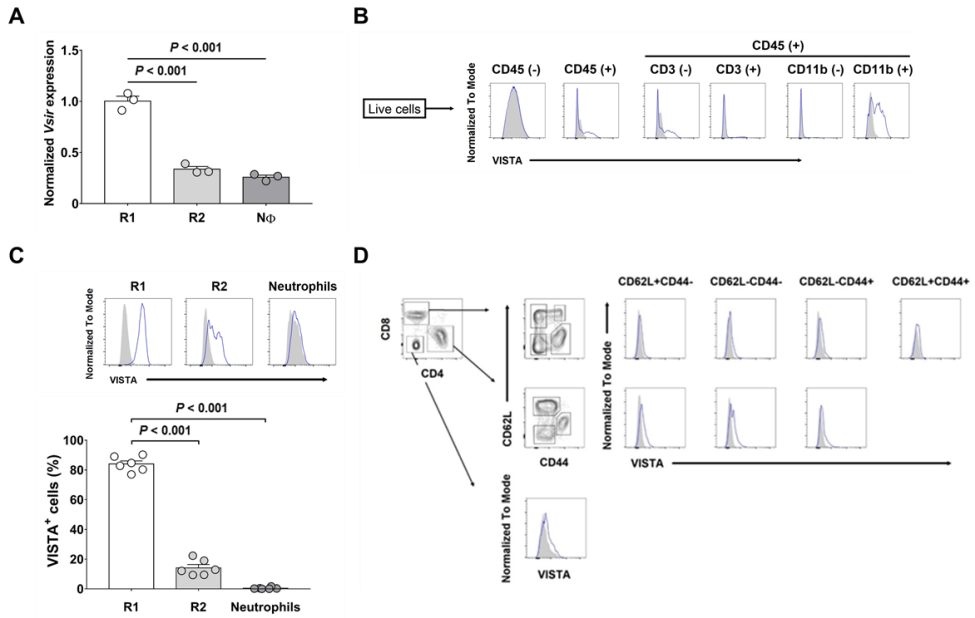

Figure 19. VISTA expression in kidney. (A) Relative *Vsir* mRNA expression in kidney macrophages (R1 and R2) and neutrophils. Results are triplicates of 3 samples per group. (B) VISTA expression in kidney immune and non-immune parenchymal cells. (C) Representative flow cytometry plot of VISTA and $VISTA^+$ cells in kidney macrophages and neutrophils. Bar graphs show the mean ± SEM. Data were combined from three independent experiments (n = 2/experiment). p-values were obtained using a two-tailed Student's t test. (D) Representative flow cytometry plot of VISTA in kidney $CD3^+$ T cells. Data (B, D) represent two independent experiments (n = 2/experiment).

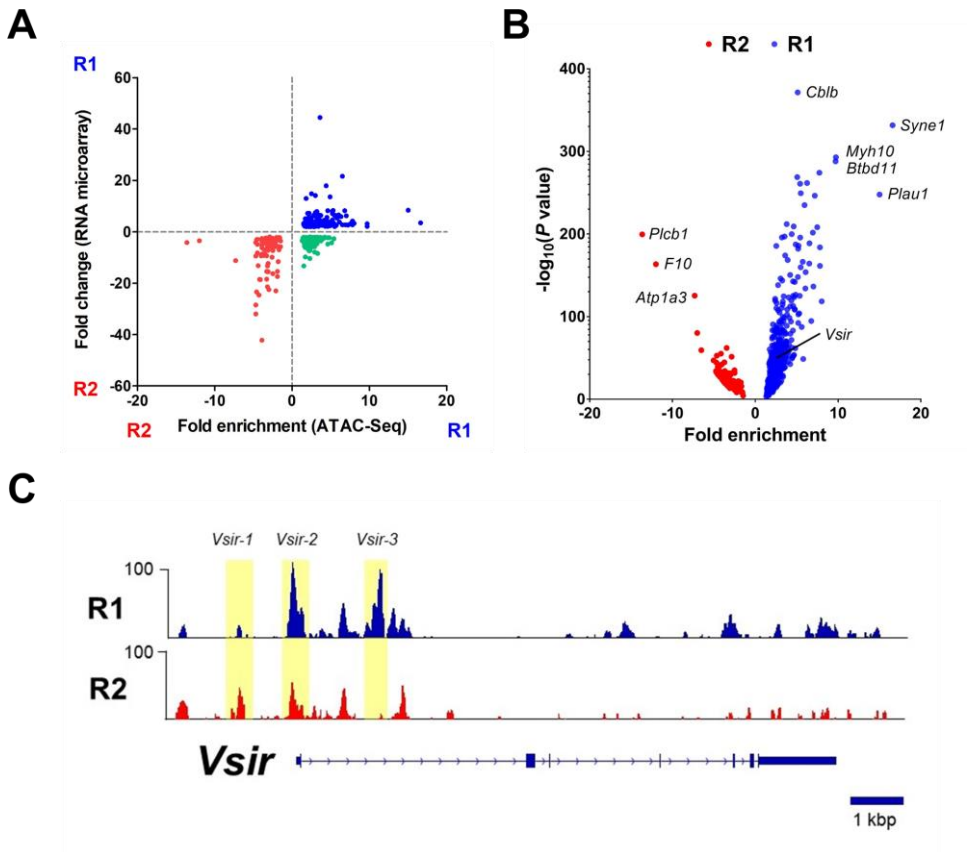

Figure 20. The chromatin in the *Vsir* gene site was more accessibility in R1 macrophages than in R2 macrophages. (A) Integrated plot of microarray and ATAC sequencing. (B) Volcano plot of ATAC sequencing of R1 and R2 macrophages. (C) Chromatin opening of the *Vsir* gene site in R1 and R2 macrophages. All results (A, B, C) are duplicates of two samples.

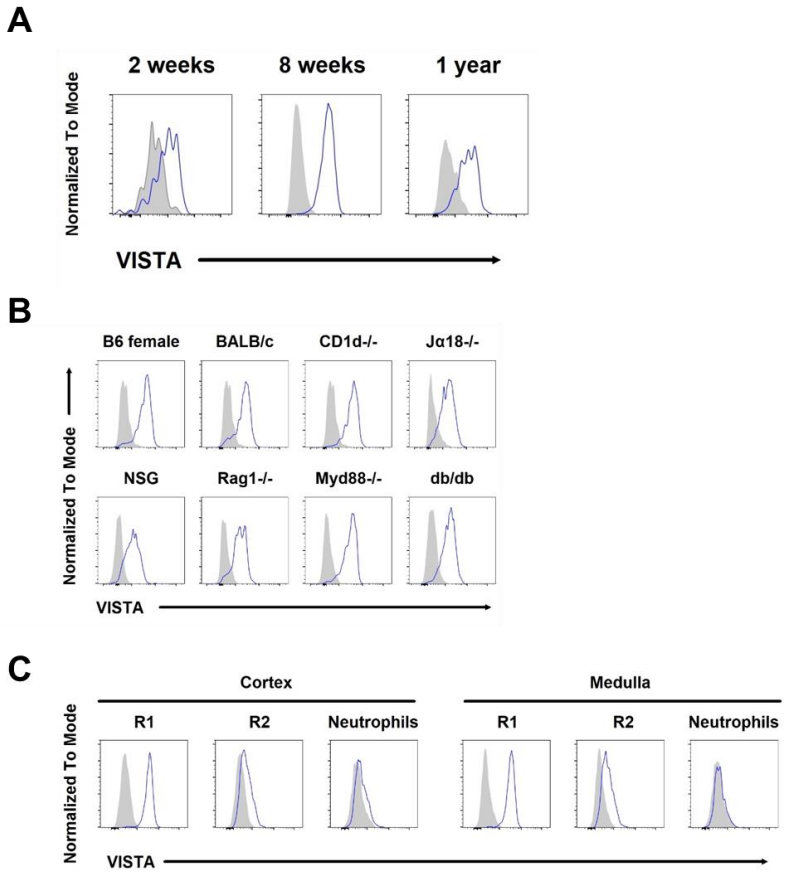

Figure 21. VISTA expression in kidney-resident macrophages did not depend on various condition. (A) VISTA expression in kidney-resident macrophages on 2 weeks, 8 weeks or 1 year B6 mice. (B) VISTA expression in kidney-resident macrophages on mouse strains. (C) VISTA expression in kidney-resident macrophages on location within the kidney. All representative flow cytometry plots from one of three independent experiments (n = 1/group/experiment) are shown. Cells were gated from the $DAPI^-$ $CD45^+$ $Ly6G^+$(Neutrophils), $DAPI^-$ $CD45^+$ $Ly6G^-$ $CD11b^{int}$ $F4/80^{high}$ (R1) and $CD11b^{high}$ $F4/80^{int}$ (R2).

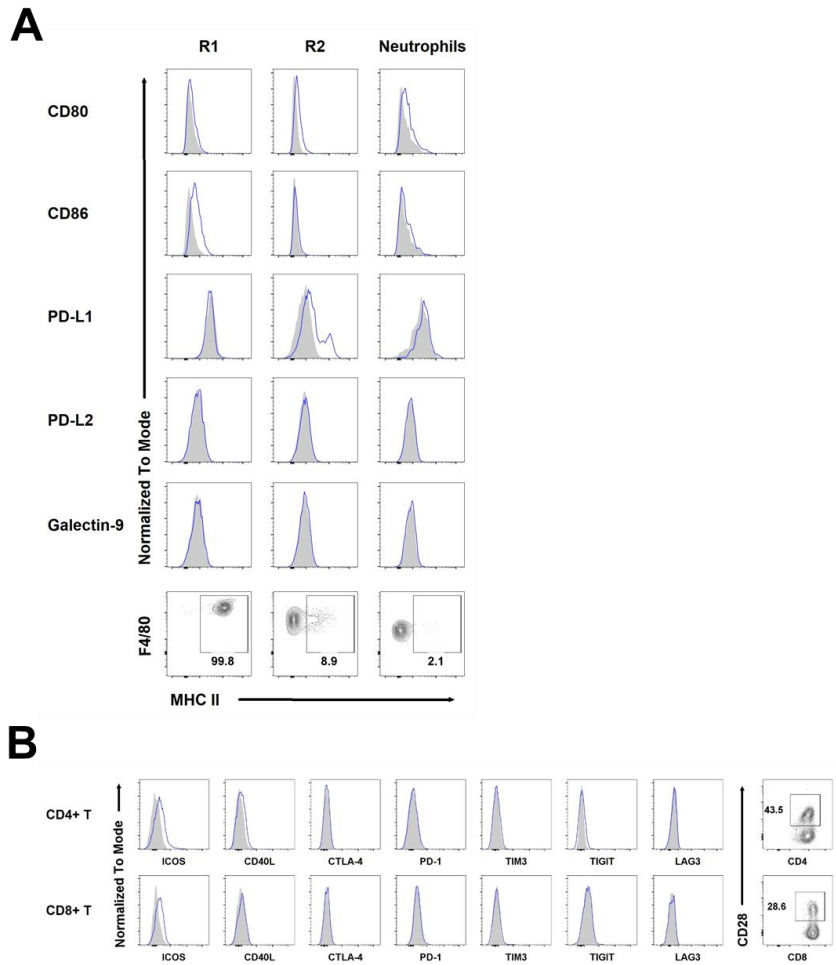

Figure 22. Expressions of immune checkpoint molecules in kidney.

(A) Expressions of immune checkpoint molecules in macrophages and neutrophils (B). Expressions of other immune checkpoint molecules in kidney $CD3^+$ T cells. All representative flow cytometry plots from one of three independent experiments (n = 1/experiment) are shown. PD-L1 or 2, Programmed death-ligand 1 or 2; ICOS, Inducible T-cell co-stimulatory; CTLA-4, Cytotoxic T-Lymphocyte Associated Protein 4; PD-1, Programmed death 1; TIM3, T-cell immunoglobulin and mucin-domain containing-3; TIGIT, T cell immunoglobulin and ITIM domain; LAG3, Lymphocyte-activation gene 3.

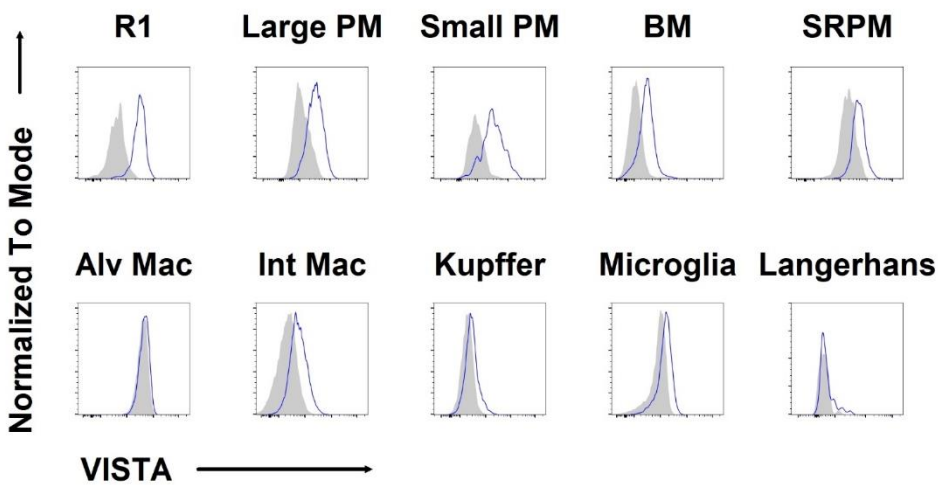

Figure 23. VISTA expression in tissue-resident macrophages. Representative flow cytometry plots from one of three independent experiments (n = 1/group/experiment). Large PM, large peritoneal macrophage; Small PM, small peritoneal macrophage; BM, bone marrow macrophage; SRPM, splenic red pulp macrophage; Alv Mac, alveolar macrophage; Int Mac, Intestinal macrophage.

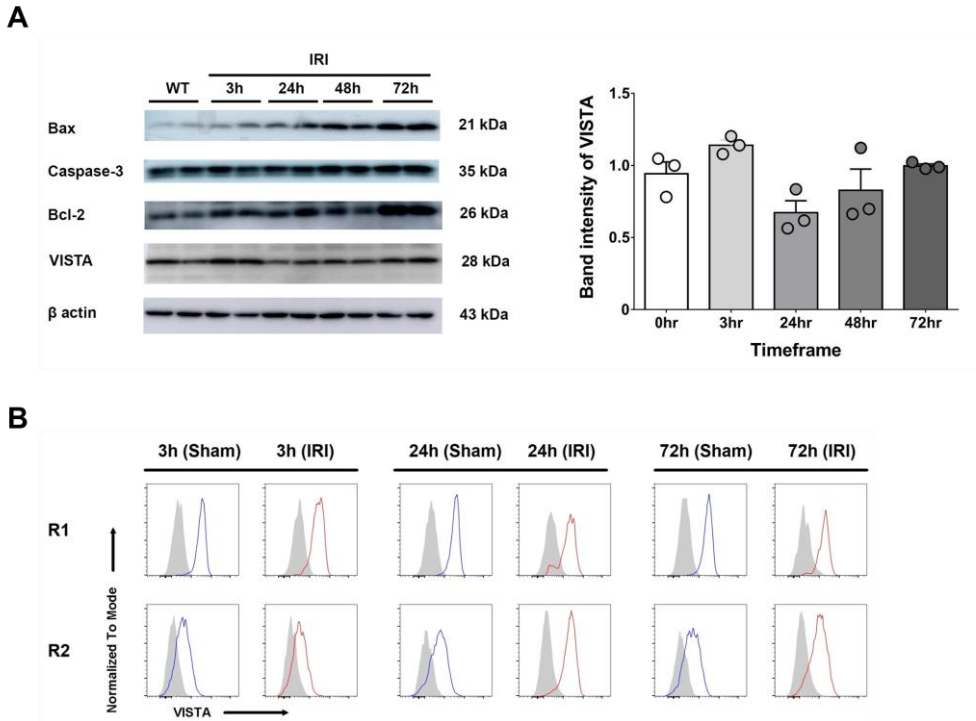

Figure 24. VISTA expression in tissue and R1 macrophages was remained elevated after ischemia reperfusion injury. (A) Expressions of VISTA and other molecules such as Bax, Caspase-3, and Bcl-2 in kidneys after ischemia-reperfusion injury (IRI). Bar graphs show the mean ± SEM. Data were combined from three independent experiments. (B) VISTA expression in R1 and R2 macrophages after IRI. Cells were gated from the $DAPI^{-}CD45^{+}Ly6G^{-}CD11b^{int}F4/80^{high}$ (R1) and $CD11b^{high}F4/80^{int}$ (R2). Representative flow cytometry plots from one of three independent experiments (n = 1/group/experiment) are shown.

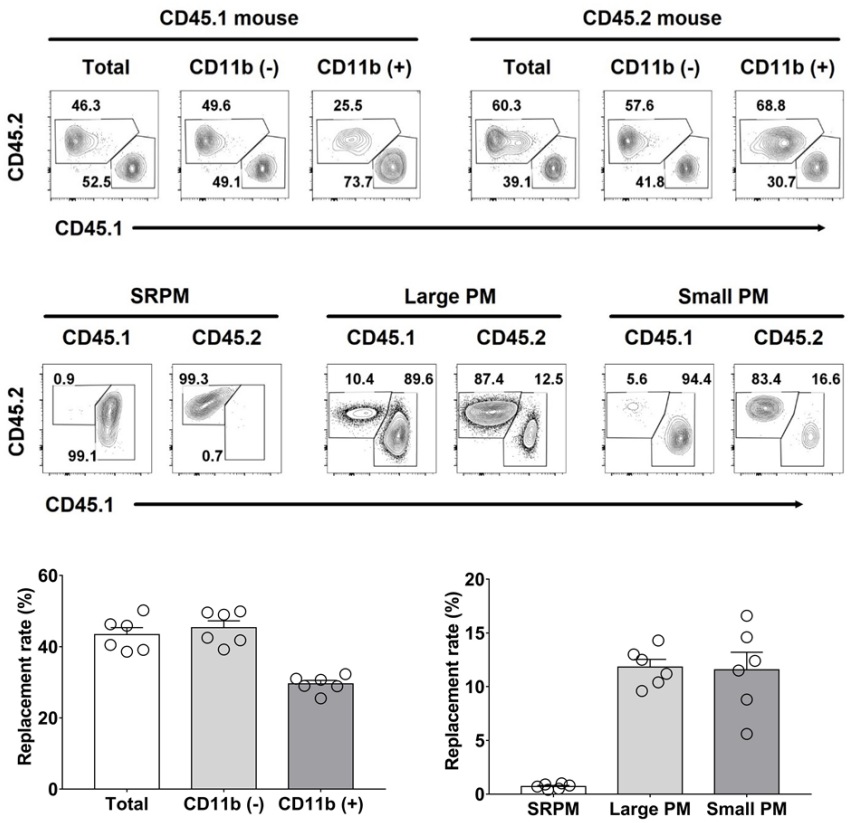

Figure 25. Replacement of resident macrophages in the peripheral blood, spleen and peritoneum at 2 months after unilateral ischemia–reperfusion injury. Peripheral blood, spleen and peritoneal cells were harvested from CD45.1 and CD45.2 congenic B6 mice joined parabiotic pairs. All data represent three independent experiments (*n* = 2/group/experiment). Bar graphs show the mean ± SEM. SRPM, splenic red pulp macrophage; PM, peritoneal macrophage.

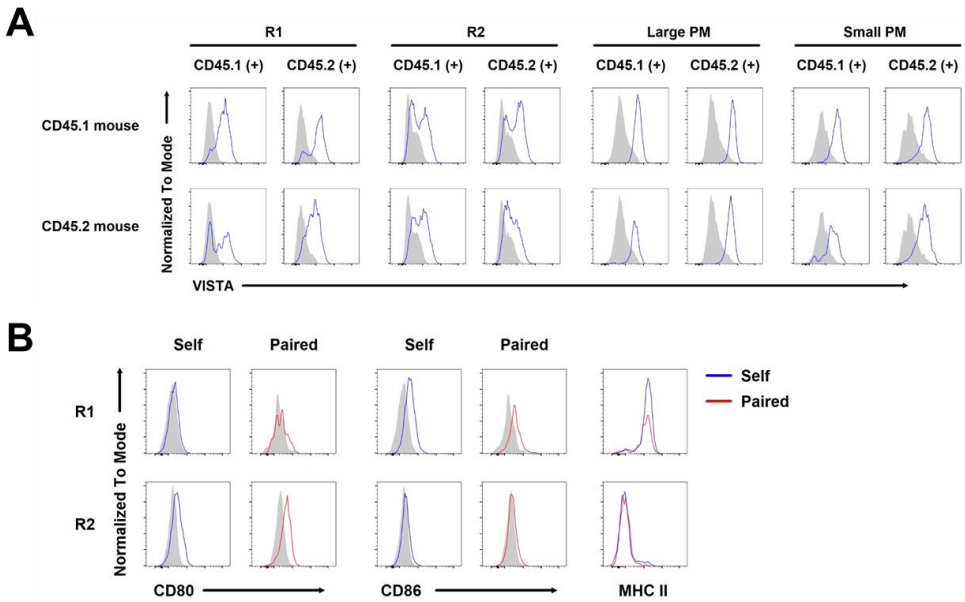

Figure 26. VISTA expression of replaced and non-replaced kidney and peritoneal macrophages in the parabiosis model. (A) VISTA expression of R1, R2, Large PM and Small PM in CD45.1 and CD45.2 congenic parabiosis model at 2 months after generation of parabiont mice. (B) Other immune checkpoint molecules in replaced and non-replaced kidney macrophages. All data (A, B) represent two independent experiments (n = 2/group/experiment).

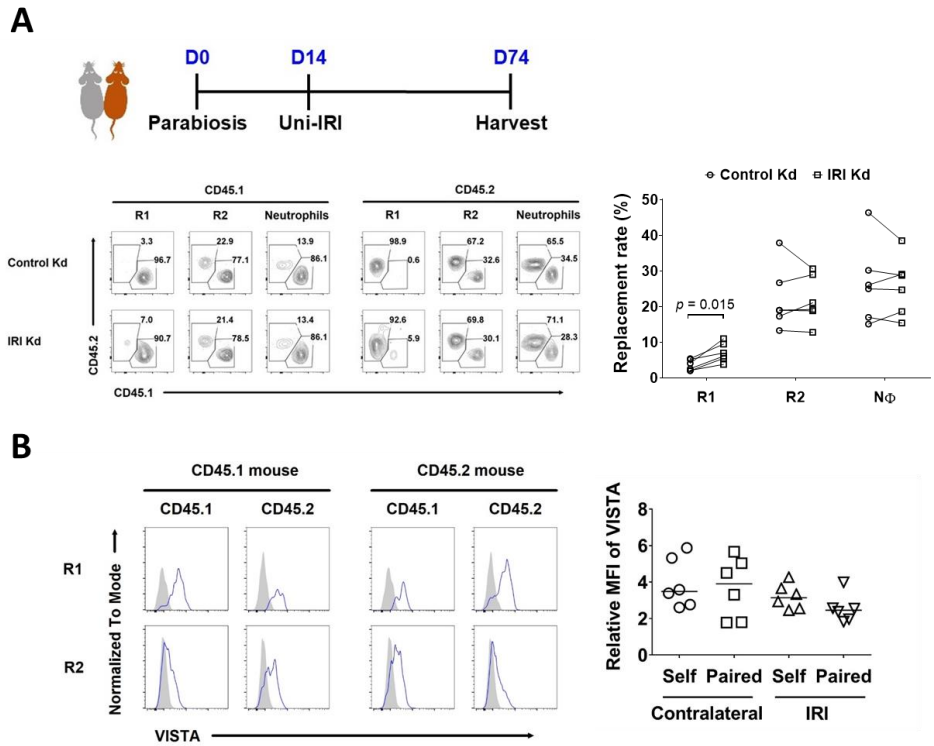

Figure 27. Replacement rate of kidney macrophages after IRI. (A) Replacement rate of kidney macrophages and neutrophils by paired parabiont cells at 2 months after IRI. (B) VISTA expression in replaced and non-replaced kidney macrophages at 2 months after IRI. All data (A, B) were combined from three independent experiments (n = 2/group/experiment). p-values were obtained using a two-tailed Student's t test.

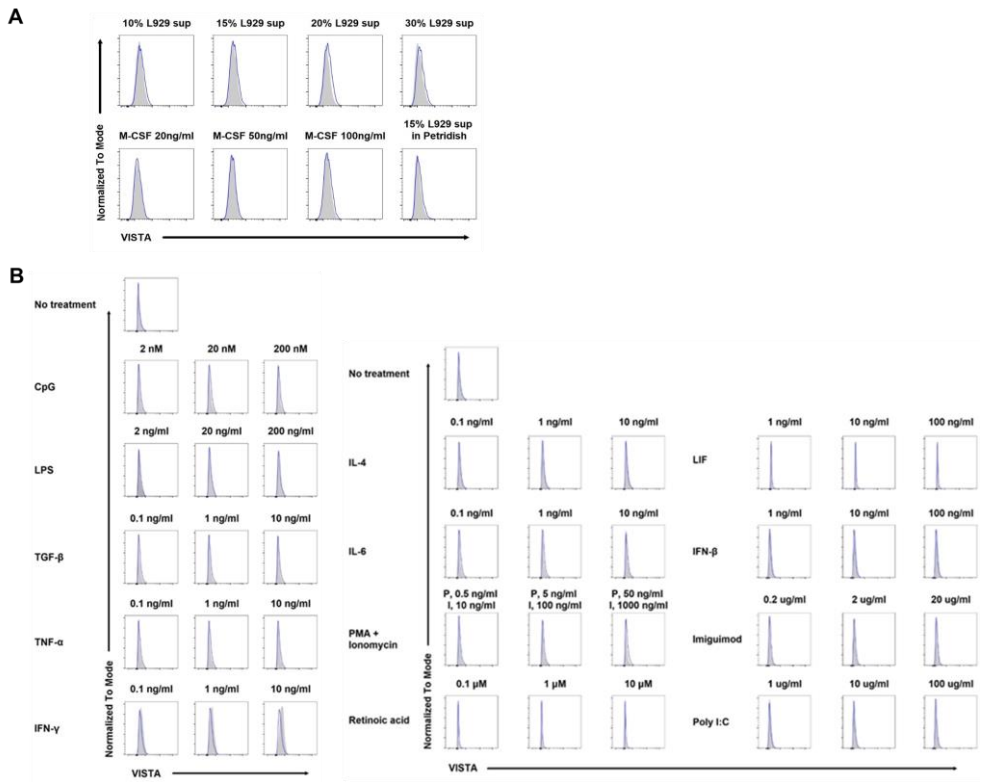

Figure 28. VISTA expression in bone marrow-derived macrophages with various condition. (A) VISTA expression in bone marrow-derived macrophages after *in vitro* culture with the indicated stimulants. (B) Effects of cytokine or stimulants on the expression of VISTA in bone marrow-derived macrophage. All data (A, B) represent three independent experiments (n = 3/group/experiment). Sup, supernatant; M-CSF, macrophage colony—stimulating factor; LPS, lipopolysaccharide; TGF-β, transforming growth factor-β; TNF- α, tumor necrosis factor-α; IFN, interferon; IL, interleukin; LIF, leukemia inhibitory factor; PMA, phorbol 12-myristate 13-acetate; poly I:C, polyinosinic-polycytidylic acid.

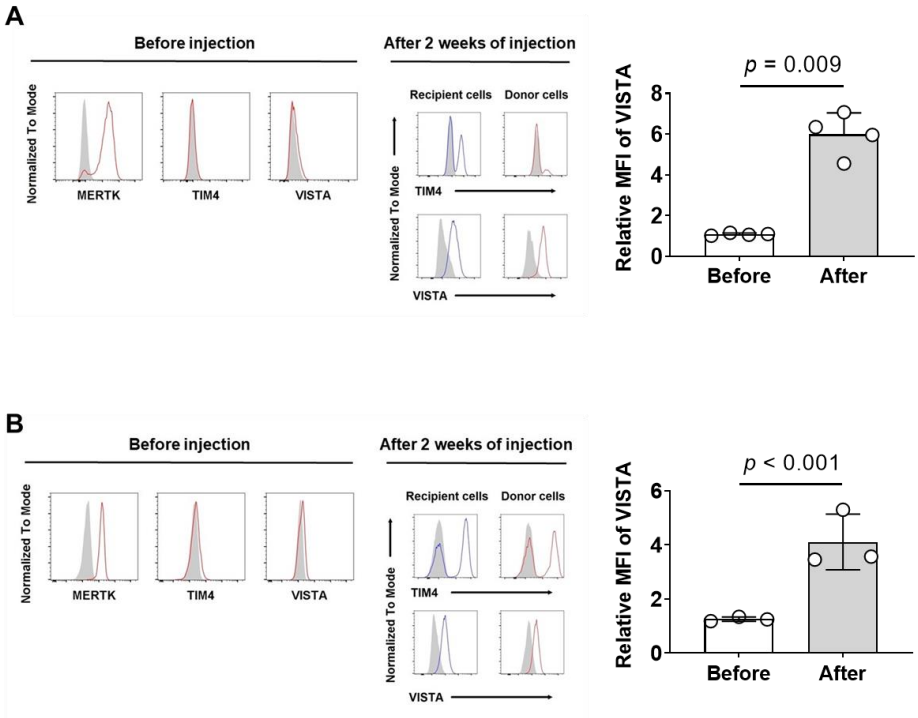

Figure 29. Tissue environment-dependent VISTA expression in kidney macrophages. (A) Restoration of VISTA expression in cultured BMDMs after residency in the peritoneal cavity after 2 weeks of injection. (B) Restoration of VISTA expression in cultured peritoneal macrophages after residency in the peritoneal cavity after 2 weeks of injection. All data (A, B) were combined from two independent experiments (n = 1~2/group/experiment). Bar graphs show the mean ± SEM. p-values were obtained using a two-tailed Student's t test.

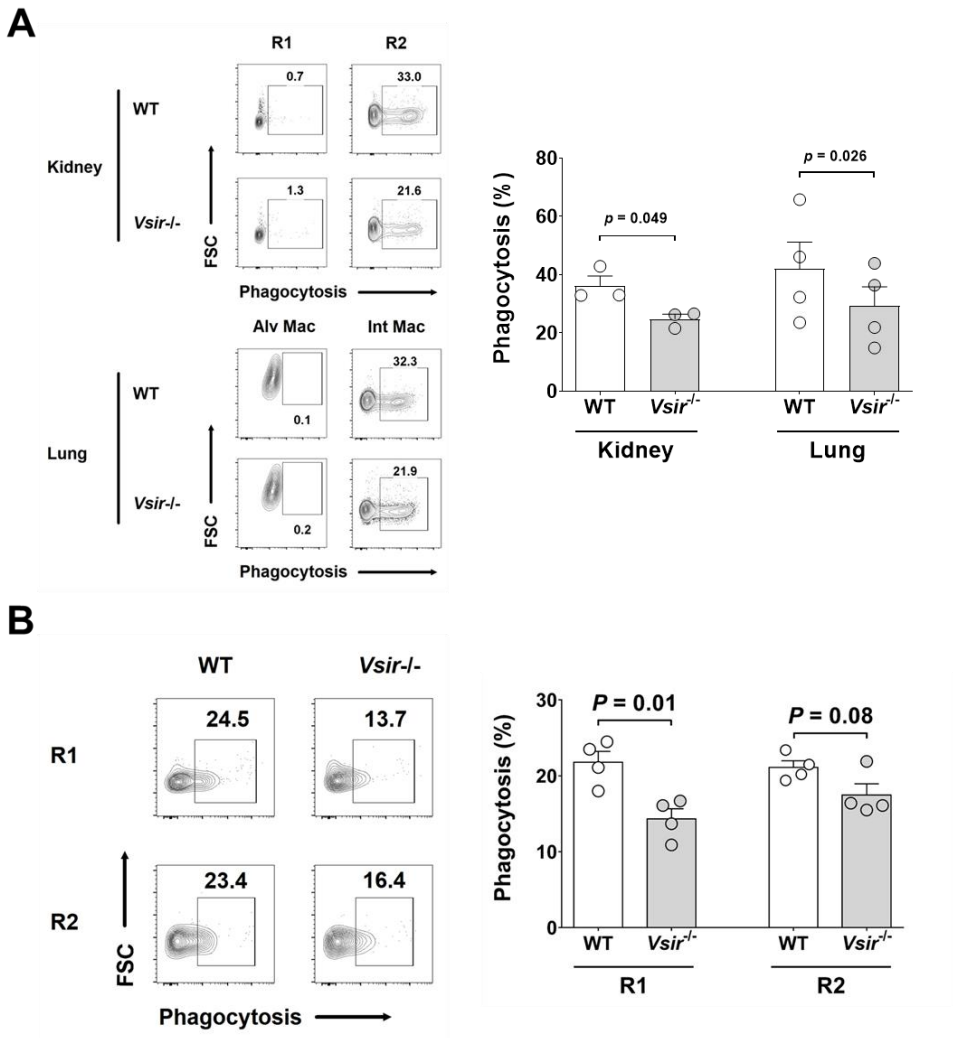

Figure 30. *In vivo* or *In vitro* phagocytic capacity of VISTA. (A) *In vivo* phagocytic capacity in wild-type and *Vsir*$^{-/-}$ mice. Lung-resident macrophages were used as the control group. (B) *In vitro* phagocytic capacity in single cell suspension assay with apoptotic cells. All data (A, B) were combined from two independent experiments (n = 2/group/experiment). Bar graphs show the mean ± SEM. p-values were obtained using a two-tailed Student's t test.

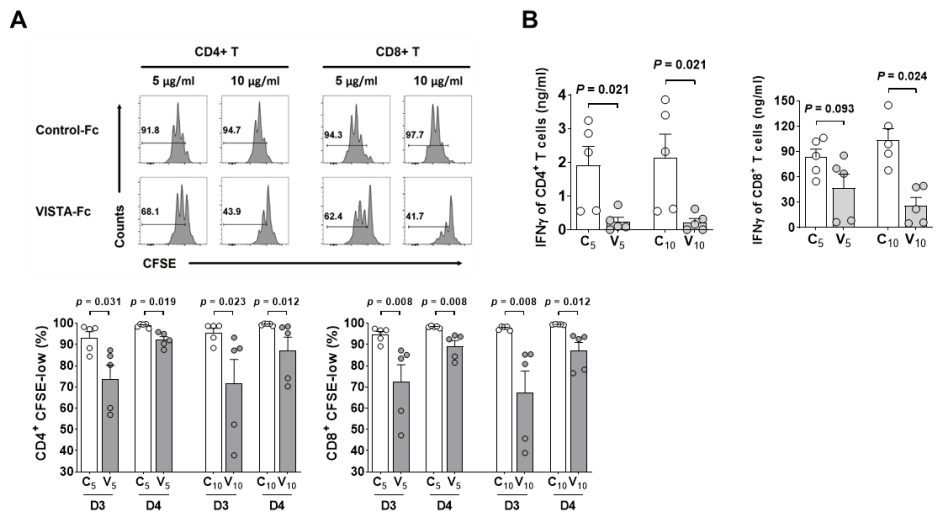

Figure 31. VISTA inhibited the activation and proliferation of naïve T cells and their IFN-γ secretion. (A) *In vitro* culture of CFSE-labeled $CD62L^{-}CD4^{+}$ or $CD62L^{-}CD8^{+}$ T cells on plates coated with anti-CD3 Abs and VISTA-Fc or control-Fc. Proliferation rates were calculated by the proportion of CFSE-low cells. Representative flow cytometry plot from one of five independent experiments. Bar graph were combined from five independent experiments (n = 1/group/experiment). (B) Amounts of T-cell IFN-γ secretion at day 3 evaluated by ELISA. Data were combined from five independent experiments (n = 1/group/experiment). Bar graphs show the mean ± SEM. p-values were obtained using a two-tailed Student's t test.

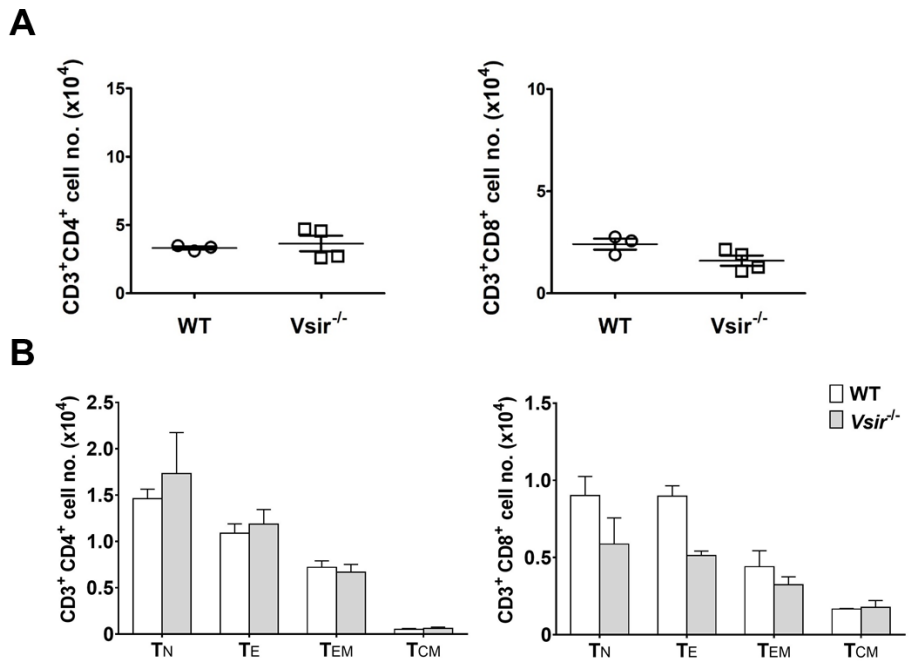

Figure 32. Baseline number of kidney T cells in *Vsir*$^{-/-}$ mice. (A) Total CD4^{+} and CD8^{+} T cells. (B) T cell subsets in normal kidneys. Bar and Bar graphs show the mean ± SEM. Cells were gated from the DAPI^{-}CD45^{+}CD3^{+}. All data (A, B) were combined from two independent experiment (n = 2/group/experiment). T_N, CD44^{-} CD62L^{+} naïve T; T_E, CD44^{-} CD62L^{-} effector T; T_{EM}, CD44^{+} CD62L^{-} effector memory T; T_{CM}, CD44^{+} CD62L^{+} central memory T.

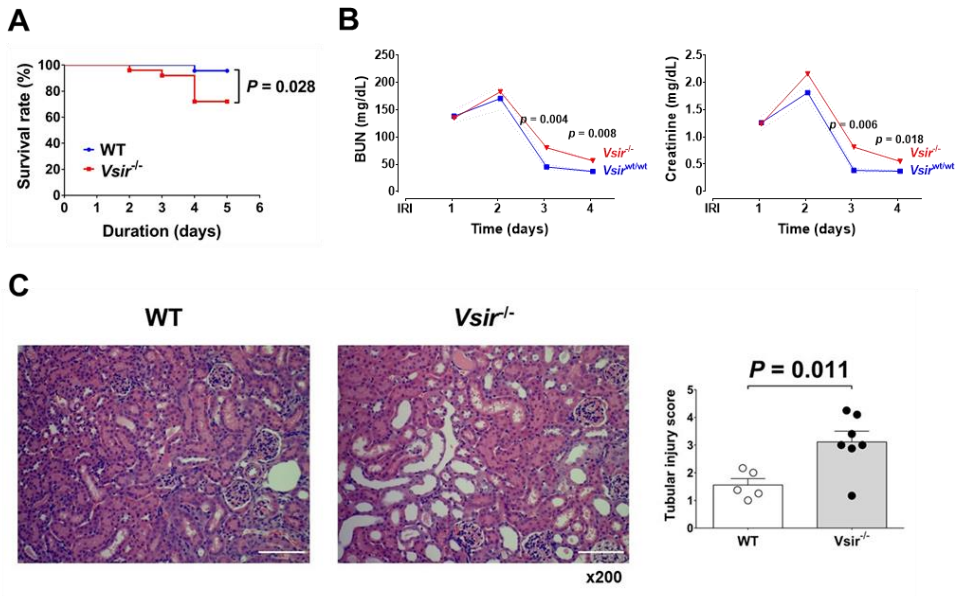

Figure 33. Loss of VISTA delayed the repair from the induction of ischemia-reperfusion injury(IRI). (A) Survival curves after the induction of IRI. (B) Kinetics of kidney injury parameters such as blood urea nitrogen (BUN) and creatinine after IRI in wild-type and *Vsir*$^{-/-}$ mice. (C) Representative H&E images at 96 h after IRI. Tubular injury score was calculated using five mice per group. Scale bar = 100 μm. All data (A, B, C) were combined from three independent experiments (n = 2~3/group/experiment). Bar graphs show the mean ± SEM. p-values were obtained using a two-tailed Student's t test.

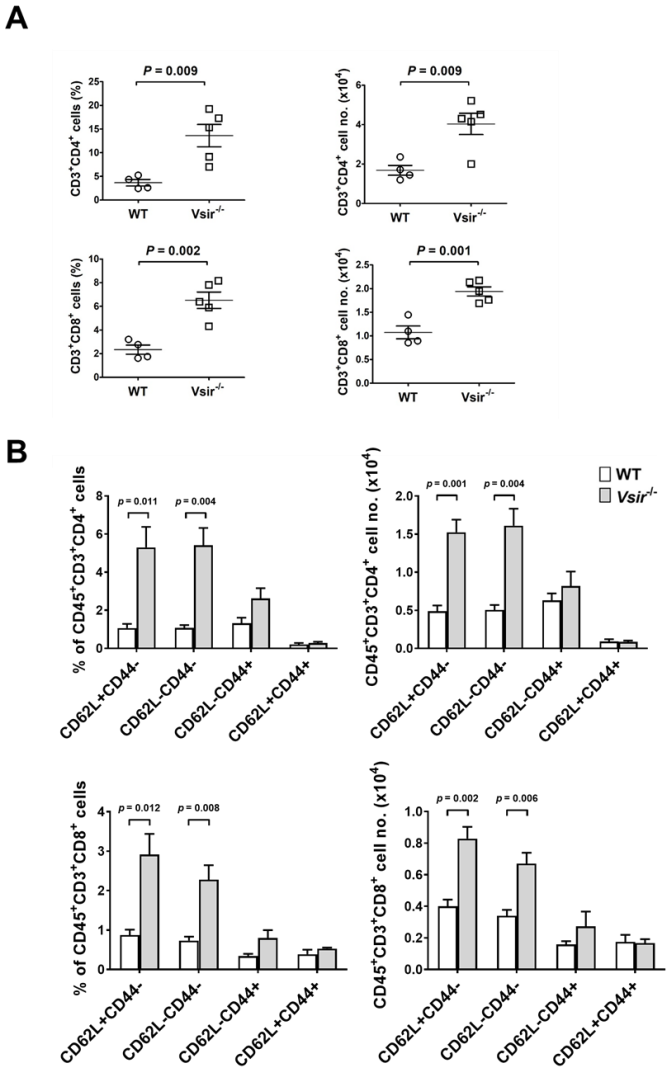

Figure 34. Loss of VISTA inappropriately regulated T cell activation and proliferation after IRI. (A)Flow cytometry analysis of kidney infiltrating T cells at 96 h after IRI. (B) Subpopulation of T cells based on the expression of CD62L and CD44 at 96 h after IRI. All data (A, B) were combined from two independent experiments (n = 2~3/group/experiment). Bars and Bar graphs show the mean ± SEM. p-values were obtained using a two-tailed Student's t test.

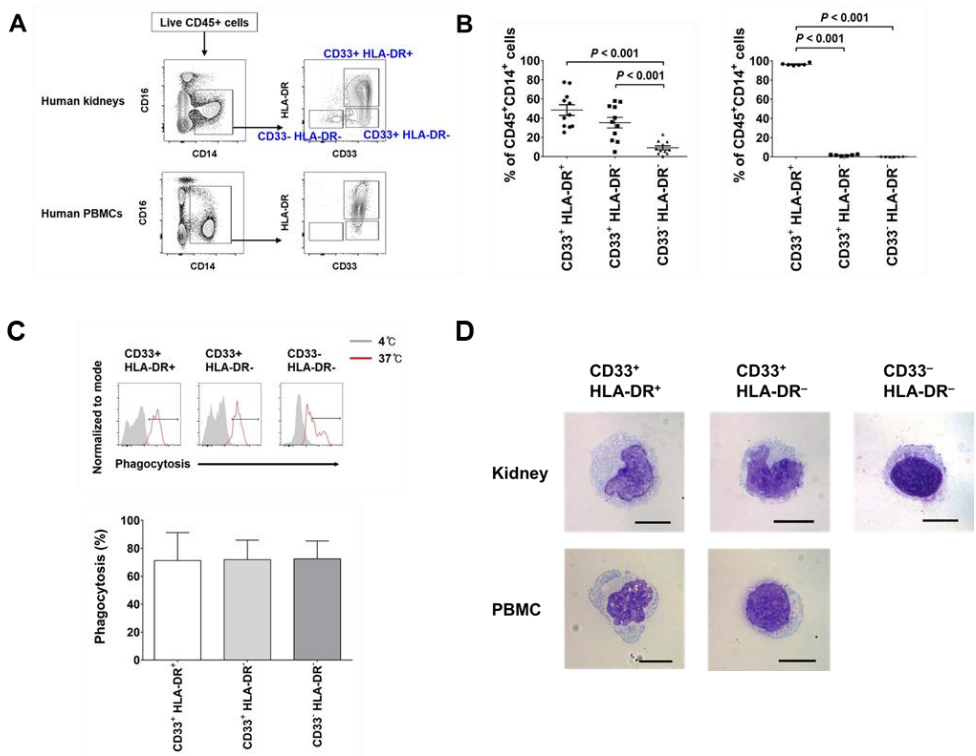

Figure 35. The characterization of human macrophages including kidney-resident macrophages. (A) Presence of $CD14^+$ myeloid cells in human kidneys (upper panel) and peripheral blood (lower panel). Cells were categorized by the expression of CD33 and HLA-DR. Representative results from one of eleven independent experiments. (B) Proportion of three myeloid cell subsets in human kidneys (left) and peripheral blood (right). Data were combined from eleven independent experiments (n = 1/experiment). Bars show the mean ± SEM. p-values were obtained using a two-tailed Student's t test. (C) Phagocytic capacity of human kidney $CD14^+$ cells in single cell suspension assay. Data represent three independent experiments (n = 1/experiment). Bar graphs show the mean ± SEM. (D) Giemsa staining of $CD14^+$ mononuclear phagocytes from human kidney and peripheral blood (×1000). Scale bar = 10 μm.

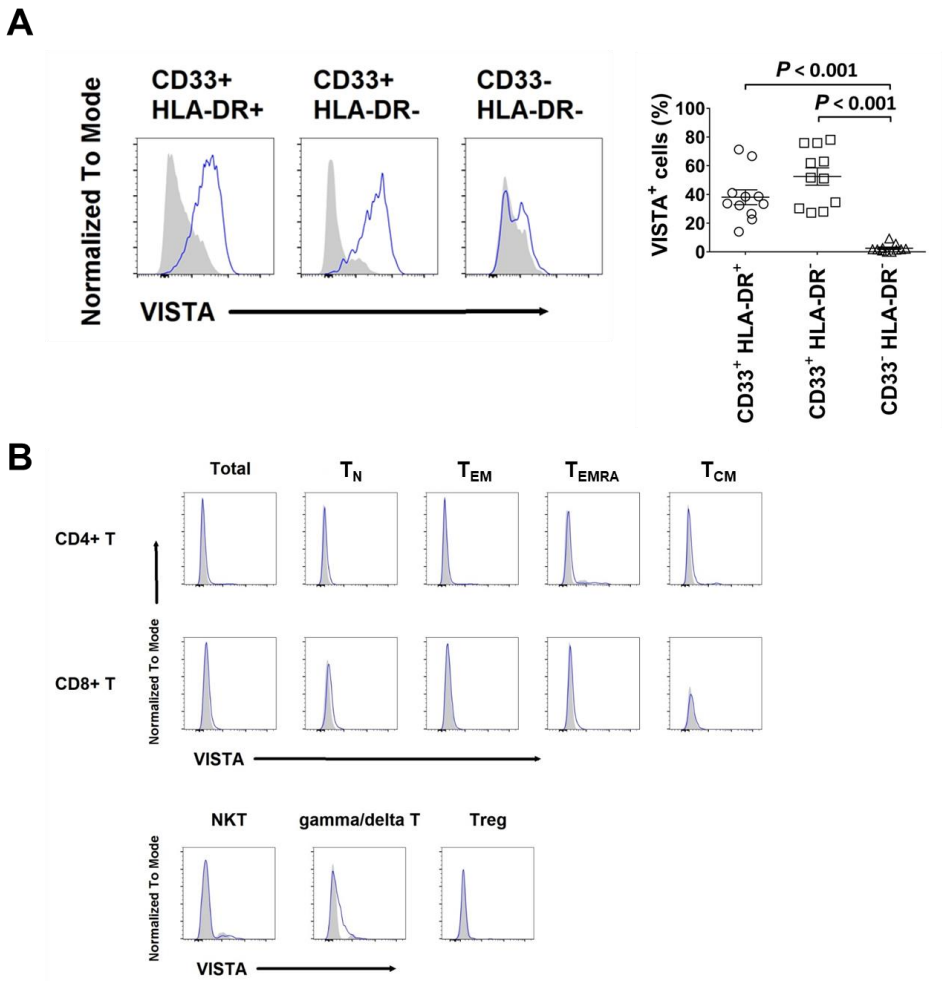

Figure 36. VISTA expression in human kidney macrophages and T cells. (A) VISTA expression in human kidney mononuclear phagocytes. Cells were gated from the $DAPI^{-}$ $CD45^{+}$ $CD14^{+}$. Data represent eleven independent experiments (n = 1/experiment). Bars show the mean ± SEM. p−values were obtained using a two−tailed Student's t test. (B) VISTA expression in human kidney. Representative flow cytometry plots from one of three independent experiments (n = 2/experiment). T_N, naïve T; T_{CM}, central memory T; T_{EM}, effector memory T; T_{EMRA}, $CD45RA^{+}$ effector memory T; Treg, regulatory T.

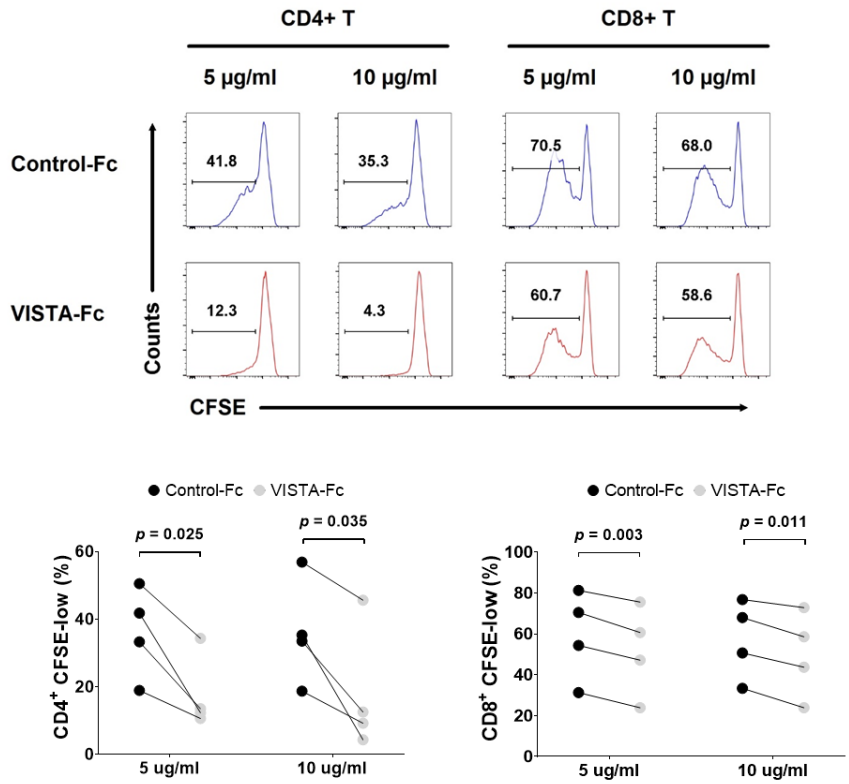

Figure 37. VISTA inhibited the proliferation of human T cells. *In vitro* culture of CFSE-labeled $CD4^+$ or $CD8^+$ human T cells on plates coated with anti-CD3 Abs and VISTA-Fc or control-Fc. Proliferation rates were calculated by the proportion of CFSE-low cells. Representative flow cytometry plots from four samples per group are shown. Data were combined from four independent experiments (n = 1/group/experiment). p-values were obtained using a two-tailed Student's t test.

Ⅴ. REFERENCES

1. Kurts, C., Panzer, U., Anders, H. J. & Rees, A. J. The immune system and kidney disease: basic concepts and clinical implications. *Nat Rev Immunol.* 2013;13:738−753.
2. Lee, V. W. *et al.* Regulatory immune cells in kidney disease. *Am J Physiol Renal Physiol.* 2008;295:335−342.
3. Cassini, M. F. *et al.* Mcp1 Promotes Macrophage−Dependent Cyst Expansion in Autosomal Dominant Polycystic Kidney Disease. *J Am Soc Nephrol.* 2018;29:2471−2481.
4. Breyer, M. D. & Susztak, K. The next generation of therapeutics for chronic kidney disease. *Nat Rev Drug Discov.* 2016;15:568−588, (2016).
5. KDIGO Clinical Practice Guideline for Glomerulonephritis. *Kidney Int Suppl*. 2012;2:142−274.
6. KDIGO 2012 Clinical Practice Guideline for the Evaluation and Management of Chronic Kidney Disease. *Kidney Int Suppl*. 2013;3: 1−150.
7. Kronbichler, A., Windpessl, M., Pieringer, H. & Jayne, D. R. W. Rituximab for immunologic renal disease: What the nephrologist needs to know. *Autoimmun Rev*. 2017;16:633−643.
8. Noble, J., Jouve, T., Janbon, B., Rostaing, L. & Malvezzi, P. Belatacept in kidney transplantation and its limitations. *Expert Rev Clin Immunol*. 2019;15:359−367.
9. Li L, Okusa MD. Macrophages, dendritic cells, and kidney ischemia−reperfusion injury. *Semin Nephrol.* 2010;30:268−277.
10. Smolders, J. *et al.* Tissue−resident memory T cells populate the human brain. *Nat Commun*. 2018;9:4593.
11. Szabo, P. A., Miron, M. & Farber, D. L. Location, location, location: Tissue resident memory T cells in mice and humans. *Sci Immunol*. 2019;4: eaas9673.
12. Stewart, B. J. *et al.* Spatiotemporal immune zonation of the human kidney. *Science*. 2019;365:1461−1466.
13. Lee SH, Charmoy M, Romano A, et al. Mannose receptor high, M2 dermal macrophages mediate nonhealing Leishmania major infection in a Th1 immune environment. *J Exp Med.* 2018;215:357−375.

14. Machiels B, Dourcy M, Xiao X, et al. A gammaherpesvirus provides protection against allergic asthma by inducing the replacement of resident alveolar macrophages with regulatory monocytes. *Nat Immunol.* 2017;18:1310−1320.
15. Zhu Y, Herndon JM, Sojka DK, et al. Tissue−Resident Macrophages in Pancreatic Ductal Adenocarcinoma Originate from Embryonic Hematopoiesis and Promote Tumor Progression. *Immunity.* 2017;47:323−338.
16. Lim HY, Lim SY, Tan CK, et al. Hyaluronan Receptor LYVE−1−Expressing Macrophages Maintain Arterial Tone through Hyaluronan−Mediated Regulation of Smooth Muscle Cell Collagen. *Immunity.* 2018;49:326−341.
17. Roberts AW, Lee BL, Deguine J, et al. Tissue−Resident Macrophages Are Locally Programmed for Silent Clearance of Apoptotic Cells. *Immunity.* 2017;47:913−927.
18. Ginhoux F, Jung S. Monocytes and macrophages: developmental pathways and tissue homeostasis. *Nat Rev Immunol.* 2014;14:392−404.
19. Varol C, Mildner A, Jung S. Macrophages: development and tissue specialization. *Ann Rev Immunol.* 2015;33:643−675.
20. Lavin Y, Winter D, Blecher−Gonen R, et al. Tissue−resident macrophage enhancer landscapes are shaped by the local microenvironment. *Cell.* 2014;159:1312−1326.
21. Hagemeyer N, Kierdorf K, Frenzel K, et al. Transcriptome−based profiling of yolk sac−derived macrophages reveals a role for Irf8 in macrophage maturation. *EMBO J.* 2016;35:1730−1744.
22. Hashimoto D, Chow A, Noizat C, et al. Tissue−resident macrophages self−maintain locally throughout adult life with minimal contribution from circulating monocytes. *Immunity.* 2013;38:792−804.
23. Stamatiades EG, Tremblay ME, Bohm M, et al. Immune Monitoring of Trans−endothelial Transport by Kidney−Resident Macrophages. *Cell.* 2016;166:991−1003.
24. Kavai M, Szegedi G. Immune complex clearance by monocytes and macrophages in systemic lupus erythematosus. *Autoimmun Rev.* 2007;6:497−502.

25. Puranik AS, Leaf IA, Jensen MA, et al. Kidney−resident macrophages promote a proangiogenic environment in the normal and chronically ischemic mouse kidney. *Sci Rep.* 2018;8:13948.
26. Mahoney KM, Rennert PD, Freeman GJ. Combination cancer immunotherapy and new immunomodulatory targets. *Nat Rev Drug Discov.* 2015;14:561−584.
27. Xu W, Hieu T, Malarkannan S, et al. The structure, expression, and multifaceted role of immune—checkpoint protein VISTA as a critical regulator of anti−tumor immunity, autoimmunity, and inflammation. *Cell Mol Immunol.* 2018;15:438−446.
28. Stroncek DF, Berger C, Cheever MA, et al. New directions in cellular therapy of cancer: a summary of the summit on cellular therapy for cancer. *J Transl Med.* 2012;10:48.
29. Wang L, Rubinstein R, Lines JL, et al. VISTA, a novel mouse Ig superfamily ligand that negatively regulates T cell responses. *J Exp Med.* 2011;208:577−592.
30. Wang J, et al. VSIG−3 as a ligand of VISTA inhibits human T−cell function. *Immunology*. 2019;156:74−85.
31. Johnston RJ, Su LJ, Pinckney J, et al. Vista is an acidic pH−selective ligand for PSGL−1. *Nature* 2019;574:565−70.
32. Liu J, et al., Immune−checkpoint proteins VISTA and PD−1 nonredundantly regulate murine T−cell responses. *Proc. Natl. Acad. Sci*. 2015;112:6682−6687
33. Le Mercier I, et al., VISTA regulates the development of protective antitumor immunity. *Cancer Res*. 2014;74:1933−1944.
34. Dallas B. Flies et al., Coinhibitory receptor PD—1H preferentially suppresses CD4+ T cell mediated immunity. *the Journal of Clinical Investigation*. 2014;124:1966−1975
35. ElTanbouly MA, et al., VISTA is a checkpoint regulator for naïve T cell quiescence and peripheral tolerance. Science. 2020;367(6475).
36. Levey, A. S. *et al.* A new equation to estimate glomerular filtration rate. *Ann Intern Med*. 2009;150:604−612.
37. Kumar, B. V. et al. Human Tissue−Resident Memory T Cells Are Defined by Core Transcriptional and Functional Signatures in Lymphoid and Mucosal Sites. *Cell Rep*. 2017;20:2921−2934.
38 Lambert, C., Preijers, F., Yanikkaya Demirel, G. & Sack, U. Monocytes and macrophages in flow: an ESCCA initiative on

advanced analyses of monocyte lineage using flow cytometry. *Cytometry B Clin Cytom*. 2017;92:180−188.

39 Stamatiades, E. G. *et al.* Immune Monitoring of Trans−endothelial Transport by Kidney−Resident Macrophages. *Cell*. 2016;166:991−1003.

40 Guerriero JL. Macrophages: Their Untold Story in T Cell Activation and Function. *Int Rev Cell Mol Biol*. 2019;342:73−93.

41. Belliere J, Casemayou A, Ducasse L, et al. Specific macrophage subtypes influence the progression of rhabdomyolysis−induced kidney injury. *J Am Soc Nephrol.* 2015;26:1363−1377.

42. Gottschalk C, Kurts C. The Debate about Dendritic Cells and Macrophages in the Kidney. *Front Immunol.* 2015;6:435.

43. Cao Q, Wang Y, Wang XM, *et al.* Renal F4/80^{+} CD11c^{+} mononuclear phagocytes display phenotypic and functional characteristics of macrophages in health and in adriamycin nephropathy. *J Am Soc Nephrol.* 2015;26:349−363.

44. Lee S, Huen S, Nishio H, *et al*. Distinct macrophage phenotypes contribute to kidney injury and repair. *J Am Soc Nephrol.* 2011;22:317−326.

45. Ferenbach DA, Sheldrake TA, Dhaliwal K, *et al. Macrophage*/monocyte depletion by clodronate, but not diphtheria toxin, improves renal ischemia/reperfusion injury in mice. *Kidney Int.* 2012;82:928−933.

46. Ceeraz S, Sergent PA, Plummer SF, et al. VISTA Deficiency Accelerates the Development of Fatal Murine Lupus Nephritis. *Arthritis Rheumatol.* 2017;69:814−825.

47. Gao J, Ward JF, Pettaway CA, et al. VISTA is an inhibitory immune checkpoint that is increased after ipilimumab therapy in patients with prostate cancer. *Nat Med.* 2017;23:551−555.

48. Yoon KW, Byun S, Kwon E, et al. Control of signaling−mediated clearance of apoptotic cells by the tumor suppressor p53. *Science.* 2015;349:1261669.

49. Berry MR, Mathews RJ, Ferdinand JR, et al. Renal Sodium Gradient Orchestrates a Dynamic Antibacterial Defense Zone. *Cell.* 2017;170:860−874 e819.

50. Haniffa M, Shin A, Bigley V, et al. Human tissues contain CD141hi cross−presenting dendritic cells with functional homology to mouse CD103+ nonlymphoid dendritic cells. *Immunity.* 2012;37:60−73.
51. Segura E, Valladeau−Guilemond J, Donnadieu MH, et al. Characterization of resident and migratory dendritic cells in human lymph nodes. *J Exp Med.* 2012;209:653−660.
52. Madariaga, M. L., Kreisel, D. & Madsen, J. C. Organ−specific differences in achieving tolerance. *Curr Opin Organ Transplant*. 2015;20:392−399.
53. Hu, W. & Pasare, C. Location, location, location: tissue−specific regulation of immune responses. *J Leukoc Biol*. 2013;94:409−421.
54. Schenkel, J. M. & Masopust, D. Tissue—resident memory T cells. *Immunity*. 2014;41:886−897.
55. Girndt, M., Sester, M., Sester, U., Kaul, H. & Kohler, H. Molecular aspects of T− and B−cell function in uremia. *Kidney Int Suppl*. 2001;78: S206−211.
56. Abolins, S. *et al.* The comparative immunology of wild and laboratory mice, Mus musculus domesticus. *Nat Commun*. 2017;8:14811.
57. Kavai, M. & Szegedi, G. Immune complex clearance by monocytes and macrophages in systemic lupus erythematosus. *Autoimmun Rev*. 2007;6:497−502.
58. Puranik, A. S. et al. Kidney−resident macrophages promote a proangiogenic environment in the normal and chronically ischemic mouse kidney. *Sci Rep*. 2018;8: 13948.
59. Zimmerman, K. A. et al. Single−Cell RNA Sequencing Identifies Candidate Renal Resident Macrophage Gene Expression Signatures across Species. *J Am Soc Nephrol*. 2019;30:767−781.
60. Levy, S. Function of the tetraspanin molecule CD81 in B and T cells. *Immunol Res*. 2014;58:179−185.
61. Stremmel C, Schuchert R, Wagner F, et al. Yolk sac macrophage progenitors traffic to the embryo during defined stages of development. *Nat Commun.* 2018;9:75.
62. Ginhoux F, Guilliams M. Tissue−Resident Macrophage Ontogeny and Homeostasis. *Immunity.* 2016;44:439−449.
63 Li, Li, Mark D Okusa. Macrophages, dendritic cells, and kidney ischemia-reperfusion injury. *Seminars in nephrology.* 2010;30:268−277.

64. Cai Y, Sugimoto C, Arainga M, et al. In vivo characterization of alveolar and interstitial lung macrophages in rhesus macaques: implications for understanding lung disease in humans. *J Immunol.* 2014;192:2821−2829.
65. Bujko A, Atlasy N, Landsverk OJB, et al. Transcriptional and functional profiling defines human small intestinal macrophage subsets. *J Exp Med.* 2018;215:441−458.
66. Chen T, Cao Q, Wang Y, *et al.* M2 macrophages in kidney disease: biology, therapies, and perspectives. *Kidney Int.* 2019;95:760−773.
67. Duffield JS. Macrophages in kidney repair and regeneration. *J Am Soc Nephrol.* 2011;22:199−201.
68. Blando J, Sharma A, Higa MG, et al. Comparison of immune infiltrates in melanoma and pancreatic cancer highlights VISTA as a potential target in pancreatic cancer. *Proc Natl Acad Sci U S A.* 2019;116:1692−1697.
82. Shi J, Hou S, Fang Q, et al. PD−1 Controls Follicular T Helper Cell Positioning and Function. *Immunity.* 2018;49:264−274 e264.
83. Read S, Greenwald R, Izcue A, et al. Blockade of CTLA−4 on CD4+CD25+ regulatory T cells abrogates their function in vivo. *J Immunol.* 2006;177:4376−4383.

Ⅵ. ABSTRACT IN KOREAN

VISTA 발현 콩팥 거주 대식세포의 신장 손상에 대한 보호기전 연구

박 준 규

콩팥 질병의 발생과 치료에 관한 면역학적 메커니즘은 마우스 연구와 임상 연구를 통해 밝혀지고 있다. 그럼에도 불구하고 콩팥에서 콩팥 거주 대식세포를 포함한 거주 면역세포의 구성과 콩팥 질환에서 콩팥 거주 면역세포가 어떤 기전을 통해 질병의 경과를 조절하는지에 대한 기본적인 이해가 부족하다. 따라서 본 논문에서는 정상 콩팥에서 마우스와 사람의 거주 면역세포의 구성을 확인하고, 그 중 콩팥 거주 대식세포가 어떤 기전으로 콩팥 질병의 경과를 조절하는지 밝히고자 했다.

조직 거주 면역세포 중 특히 조직 거주 대식세포는 조직이나 기관이 특정 기능을 수행하는 데 필요한 세포 수, 형태, 혈관신생 등을 일정 상태로 유지하는 조직 항상성 조절과 면역세포에 의한 염증반응 중 특히 T 세포 활성 조절에 핵심적인 역할을 수행한다는 것이 보고되었다. 사람과 마우스 콩팥 거주 면역세포의 구성을 확인하기 위해서 콩팥 적출 수술을 받은 요로성 악성 종양 환자로부터 병변이 없는 콩팥 조직을 얻어 분석하고, 정상 마우스의 콩팥 거주 면역세포를 분석했다. 그 결과 사람 콩팥 거주 면역세포에서 $CD3^+$ T 세포는 47% ± 12% 비율을 차지했으며, 그중 $CD4^+$ T 세포와 $CD8^+$ T 세포는 각각 44% 와 56% 비율을 차지했다. 전체 $CD3^+$ T 세포에서 효과 기억세포 표현형($CCR7^-CD45RA^-CD69^-$) T 세포는 47% ± 15% 비율을 차지하며, 거주 기억세포 표현형($CCR7^-CD45RA^-CD69^+$) T 세포는 48% ± 19% 비율을 차지했다. 전체 콩팥 거주 면역세포 중 콩팥

거주 골수성세포는 10% 비율을 차지했으며, 그중 콩팥 거주 대식세포가 대부분을 차지했다. 마우스 콩팥에서 전체 콩팥 거주 면역세포 중 콩팥 거주 대식세포가 50% 비율을 차지했으며, $CD3^+$ T 세포는 20% 비율을 차지했다. 마우스와 사람 모두 콩팥 거주 대식세포는 골수성세포 중 높은 비율을 차지하는 것을 확인했다.

다음으로 허혈성 콩팥 손상에서 콩팥 거주 대식세포가 어떤 기전으로 질병의 경과를 조절하는지 분석했다. 마우스 허혈성 콩팥 손상 모델에서 클로드로네이트 리포좀을 처리해 콩팥 거주 대식세포를 선별적으로 제거한 결과 콩팥 손상에 대한 회복이 지연되는 것을 확인했다. 또한, 마우스와 사람의 콩팥 거주 대식세포는 면역관문물질로 잘 알려진 V-domain Ig suppressor of T activation (VISTA)을 지속적으로 높게 발현하고 있는 것을 확인했다. VISTA 결핍 마우스를 이용해 콩팥 거주 대식세포가 VISTA 를 통해 사멸 세포의 제거와 T 세포의 활성을 조절하는 것을 간접적으로 확인했으며, VISTA 결핍 마우스에서 허혈성 콩팥 손상에 대한 회복이 지연되는 것을 확인했다.

결론적으로 콩팥 조직 내 거주 면역세포의 전반적인 분포를 확인했으며, VISTA 를 발현하는 콩팥 내 거주 대식세포는 콩팥 조직 내에서 죽은 세포를 제거하거나 T 세포의 활성을 억제함으로 콩팥 손상 이후 회복기전에 관여한다는 것을 밝혔다.

주요어 : 콩팥, 염증반응, 조직 거주 대식세포, T 세포, 골수성세포, VISTA
학 번 : 2016-26385